Responses to referee 1 (Felix M. Schneider)

Manuscript SE-2018-102

A Multi-Technology Analysis of the 2017 North Korean Nuclear Test

Peter Gaebler, Lars Ceranna, Nima Nooshiri, Andreas Barth, Simone Cesca, Michaela Frei, Ilona Grünberg, Gernot Hartmann, Karl Koch, Christoph Pilger, J. Ole Ross, and Torsten Dahm

---

Dear Felix Schneider,

thank you very much for taking the time and interest to deliver this very thorough and constructive review of our manuscript. We carefully studied your comments and made changes and corrections to the manuscript where necessary. We hope our changes and and corrections are sufficient to make our article suitable for publication soon. Your comments and suggestions certainly helped to improve quality and clarity of the paper.

Respones to your comments are given in the following pages. Changes made in the manuscript related to your comments are given in green color, changes by the authors after re-reading the manuscript are given in grey color. Changes related to the second referee are given in blue color. Page and line numbers refer to the originally submitted manuscript.

Thank you again,
best regards

Peter Gaebler and co-authors

---

0 Abstract

0.1 COMMENT: page 1 line 9: Do you mean Seismological investigations of depth phases? Then it must be 0.6 km below surface instead of 0.8 km (otherwise it is in contradiction with the results in 2.2). In this case I would include "of depth phases" as well in the text.

RESPONSE: Thank you for this comment. First of all, you are correct, it must be 0.6 km instead of 0.8 km. We chose not to include the word depth phases here, as the sentence is not only about depth estimation using depth phases but also about epicenter estimation using regional seismic phases. We therefore used the umbrella term *seismological investigations*.

CHANGES IN THE MANUSCRIPT: page 1 line 9: changed 0.8 km to 0.6 km.

0.2 COMMENT: page 1 line 16: ehance → enhance.

RESPONSE: Typo corrected.

CHANGES IN THE MANUSCRIPT: page 1 line 16: ehance → enhance.

1 Introduction

1.1 COMMENT: page 2 line 9: It was opened → CTBT was opened (since in the sentence before you talk about CTBT and CTBTO).

RESPONSE: Changed the sentence as suggested.

CHANGES IN THE MANUSCRIPT: page 2 line 9: It was opened → CTBT was opened.

1.2 COMMENT: page 2 line 10: Place a comma after *At the time of this study.*

RESPONSE: Added comma as suggested.

CHANGES IN THE MANUSCRIPT: page 2 line 10: added comma after *At the time of this study.*

1.3 COMMENT: page 3 line 11-25: Paragraph should be resorted and corrected (shift one sentence and 3 typos).
(a) teleseimsic → teleseismic.
(b) *Radionuclide monitoring demonstrates the importance of atmospheric transport modelling (ATM) to avoid over-interpretation of variations in 133Xe concentrations.* Place this after *... effects at the surface.*
(c) at the test site, → at the test site.
(d) *The event depth is estimated for the first time by a joint inversion of source time function (STF) and depth phase waveform modeling observed at small aperture, high-frequency arrays in teleseimsic distances.* This phrase has to be modified. You do not invert the depth phase waveform modeling. You do joint inversion of the STF and the waveform composition of direct and depth phase to retrieve the depth.
(e) Additionall → Additional.

RESPONSE:
(a) Typo corrected.
(b) Shifted the sentence as suggested.
(c) Typo corrected.
(d) We would like to appreciate this point. We performed a joint inversion of the waveform composition of the source time function (STF) and direct and surface-reflected phases to retrieve the depth. We agree that this should be further clarified in the manuscript. In accordance to the reviewers comment, we modified the phrase in the revised manuscript.
(e) Typo corrected.

CHANGES IN THE MANUSCRIPT:
(a) page 2 line 17: teleseimsic → teleseismic.
(b) shifted the sentence from page 2 line 12 to page 2 line 23.
(c) Replaced comma by point on page 2 line 21.
(d) Rephrased the sentence starting with *The event depth...* on page 2 line 16.
(e) Additionall → Additionally.

2 Seismological Investigations

2.1 Epicenter Location

2.1.1 COMMENT: page 4 line 15: I do not understand the relevance of Figure 2 for the described analysis. It shows the similarity of the events. owever, as input parameter for the double difference method one needs the lag times. It would be good to find a way to show the lag time data, for the different events,

maybe in a similar way as the correlation coefficient is shown.

RESPONSE: Figure 2 illustrates the results of the correlation, which are described on page 4 lines 7-14 above the figure. The correlation results are relevant for the relative location procedure for two reasons: (1) Estimation of the time lag, as described on page 4 lines 16-18. (2) Selection of the reliable event pairs, for which a threshold of the correlation value was set. The second topic is not yet explained in the text. A corresponding statement will be included. We feel that showing lag time data for the different events is not adding that much of valuable information.

CHANGES IN THE MANUSCRIPT: page 4 line 16: Made changes to the sentence starting with *Time lags of the....*

2.2 Estimation of Hypocenter Depth and Seismic Moment

2.2.1 COMMENT: page 4 line 29: *The analysis of the time lag of near-source, surface-reflected P-phases, so-called depth phases, can potentially help in such a case, because they only depend on the depth and the P-wave velocity inlayer above the source.*
(a) I found this explanation misleading. In teleseismic distances one cannot resolve a depth phase or a depth phase lag time in the seismograms. And looking at your array beams one cannot identify any separated depth phase, since the source time function is much longer than the lag time. What you are doing is modeling the wavelet under the assumption that is consist of source time function (STF) and an reflected phase, which resembles the inverted and time shifted STF. However, in the paragraph it sounds like you are able to identify the depth phases by applying beamforming.
(b) A very similar approach as been applied in the section ARRAY BEAM MODELING of Cesca et al (2017). Please cite it here. In that publications of the 2016 nuclear explosion, arrays from different azimuths had been used (ASAR, GERES and PDAR). Why those data were not utilized for the inversion shown in this paper?

RESPONSE:
(a) The reviewer raised a very valid point. It is difficult to constrain the depth of a shallow source without a close station within a focal depths distance from the source. For a more precise estimation of the source depth, we performed a wavelet modelling composed of the direct and surface-reflected P phase and STF. We identified the direct and depth phases using the ray-tracing through the assumed velocity model used to compute the Greens Functions and select a time window around the theoretical arrival times for those phase. To support the referees assertion, we modified the text in the revised paper.
(b) We appreciate this comment. We modified the text and added citation to Cesca et al. (2017). The nuclear explosion is very short in time, and STF inversion for such procedure needs high-quality signals with very good signal-to-noise ration. We also tested the robustness of our method in terms of its independence from the azimuthal coverage of the data set used. By considering these items, we utilized the data set reported in the paper, which is different from the one used in Cesca et al. (2017).

CHANGES IN THE MANUSCRIPT:
(a) Page 4 line 26-30: Modified the sentences.
(b) Reference Cesca 2017 added.

2.2.2 COMMENT: page 5 figure 3:
(a) The figure is not displayed right in the SE-manuscript (se-2018-102.pdf). However I found a proper displayed one in se-2018-102-manuscript-version1.pdf. Please make sure, that it is right in the final version.
(b) It would be good to show the residual fit to deeper depths, since it seems like the residual decreases again from 900 to 1000m. Also 2 km is the depth estimate from MTI and this result should be in the

range of the refined method. So best would be to show the residual curve down to at least 4 km.

RESPONSE:
(a) Replaced the figure that is displayed right in the final version of the manuscript.
(b) We followed the referees suggestion and changed the figure accordingly. In the new figure, the residuals curve has been shown for deeper sources as much as our pre-computed Greens Function data base makes it possible. For sources deeper than 1500 m, we have to recalculate the GreensFunctions for all arrays used, which is computationally time consuming. We hope that the referees is convinced that the residuals increase by increasing source depth. The jump seen at depth 1000 m can be because of the velocity discontinuity (e.g. layer interface) at exactly this depth in the velocity model used for waveform modelling.

CHANGES IN THE MANUSCRIPT:
(a) Figure should be displayed correctly now.
(b) Figure adjusted as suggested.

2.2.3 COMMENT: page 5 line 5: What is the best moment tensor solution? How is it determined? Is it the solution derived later in Section 2.3? Please clarify in the text.

RESPONSE: The best moment tensor solution is the one derived in Section 2.3. To clarify this, we modified the text.

CHANGES IN THE MANUSCRIPT: page 5 line 5: Added the text *described in Subsection 2.3.*

2.2.4 COMMENT: page 5 line 6: The abbreviation STF is used only in the introduction. For better readability I would define it here again as source time function (STF).

RESPONSE: We decided to avoid abbreviations in the abstract and then introduce them the first time they are mentioned. For consistency we would rather keep it that way. The term STF is already mentioned in the Introduction section.

2.2.5 COMMENT: page 5 line 12ff: *It is assumed that all moment tensor components M_{jk} have the same time dependency, which is described as normalized STF $m(t)$ with $m(t \rightarrow \infty) = 1$. The waveform of far-field displacement pulses are controlled by the time derivative of $m(t)$, which is declared as moment rate function $\dot{m}(t)$. The P-wave from an earthquake $\dot{m}(t)$ has a single-sided pulse.*
(a) In the figure caption of Fig.3 you call m(t) moment function. Here you call it normalized STF. Please be consistent.
(b) Please give a citation for this statemement: *The waveform of far-field displacement pulses are controlled by the time derivative of m(t).*
(c) Please give a citation for this statemement: *The P-wave from an earthquake, m(t) has a single-sided pulse.*

RESPONSE:
(a) Thanks for the insightful comment. To keep the text consistent, we reviewed the paper and called m(t) moment function in the entire manuscript.
(b) The statement has been slightly modified and Dahm and Krüger (2014) was cited to support the statement.
(c) Same citation as above (2.2.5b) was provided for the statement raised in the comment.

CHANGES IN THE MANUSCRIPT:
(a) page 5 line 13: STF → moment function.
(b) page 5 line 15: Citation Dahm and Krüger 2014 added.
(c) page 5 line 15: Citation Dahm and Krüger 2014 added.

2.2.6 COMMENT: page 5 line 16: Green function → Green's function (2 times).

RESPONSE: Thanks for the comment, corrected all Green to Green's.

CHANGES IN THE MANUSCRIPT: page 5 line 16: Green function → Green's function (2 times).

2.2.7 COMMENT: page 5 line 23: The convolution in (3) equated and written in discrete form − > The convolution in (3) can be written in discrete form.

RESPONSE: Changed as suggested.

CHANGES IN THE MANUSCRIPT: page 5 line 23: The convolution in (3) equated and written in discrete form → The convolution in (3) can be written in discrete form.

2.2.8 COMMENT: page 6 line 5,7,9: Green function − > Green's function.

RESPONSE: Corrected, again thanks for the comment.

CHANGES IN THE MANUSCRIPT: page 6 lines 5,7,9: Green function → Green's function.

2.2.9 COMMENT: page 6 line 11f:
(a) Insert CRUST2.0 before Bassin et al., 2000.
(b) *Intrinsic attenuation for P-waves is set to 5000, since otherwise high frequencies are damped out at teleseismic distances.* Is this realistic? Please comment why you are allowed to do that. If not the question arises, what are you inverting for?
(c) The grid search depth phase modeling has been applied previously to different cases of induced seismicity (Dahm et al., 2007), but the simultaneous STF inversion is implemented for the first time. → The grid search depth phase modeling has been applied previously to different cases of induced seismicity (Dahm et al., 2007) and the 2016 nuclear explosion (Cesca et al. 2017), but the simultaneous STF inversion was implemented for the first time in this study.

RESPONSE:
(a) Thanks for the comment. We simply forgot this statement.
(b) We support the referees assertion, but we do not see a problem if the quality factor is unrealistically high in the modelling. This is because the waveforms are really unaffected when propagating up and down in the uppermost mantle. However, if the quality factor is too small, high frequency content is very difficult to observe at teleseismic distances.
(c) Changed as suggested.

CHANGES IN THE MANUSCRIPT:
(a) page 6 line 11: Added CRUST 2.0 in the manuscript before the citation of Bassin et. al, 2000.
(b) No changes in the manuscript.
(c) page 6 line 12-14: Changed sentence as suggested.

2.2.10 COMMENT: page 6 line 20ff:
(a) Such an overshoot is not expected for the rupture process of tectonic earthquakes, but commonly observed for nuclear explosions. → Such an overshoot is not expected for the rupture process of tectonic earthquakes, where the moment rate and moment functions of the P-wave are single sided pulses and monotonously increasing functions, respectively. For nuclear explosions, however, this feature is commonly observed.
(b) It can be explained → This can be explained.
(c) high-frequency mb estimates in Subsection 2.4 → high-frequency mb estimates which emerged during the magnitude estimation described in Subsection 2.4.

RESPONSE:
(a) Changed as suggested.
(b) Changed as suggested.

(c) Changed as suggested.

CHANGES IN THE MANUSCRIPT:
(a) page 6 line 21: Sentence changed as suggested.
(b) page 6 line 22: It can be explained → This can be explained.
(c) page 6 line 26: high-frequency mb estimates in Subsection 2.4 → high-frequency mb estimates which emerged during the magnitude estimation described in Subsection 2.4.

2.3 Moment Tensor Inversion of the Test and the Main Aftershock

2.3.1 COMMENT: page 7 line 11: *The best solution, found at a depth of around 2 km, has a scalar moment of 2.33x1017 Nm,equivalent to a MW of 5.55.* This is inconsistent with section 2.2, where the best depth is at 600 m. Comment on that.

RESPONSE: The estimation of the centroid depth by moment tensor inversion (2 km) has a lower resolution than the hypocentral depth discussed in Section 2.2 (0.6 km). The centroid depth result may also depend on the velocity model used, as shown in Cesca et al. (2017) for the study region. In this work we use one preferred velocity model and found good waveform fits for centroid depths varying between 0 km and 2.5 km. Considering the lower resolution of centroid depth, this corresponds well with the hypocentral depth estimated be analysis of depth phases of 400-800 m (section 2.2). We improve the text to explain the differences among hypocentral and centroid depth estimates.

CHANGES IN THE MANUSCRIPT: page 7 line 11: Added the sentence *The centroid depth is poorly resolved and good waveform fits are found for very shallow sources down to 2.5 km. This result confirms the very shallow depth of 400-800 m accurately resolved by the analysis of depth phases in Subsection 2.2.*

2.3.2 COMMENT: page 7 figure 5: How the shown wave forms are selected? Do you only show those stations where the fit is good? Why do you show less wave forms in Fig. 7 compared to Fig. 5? It would be good to show the same example stations in both cases or explain why you select the given stations. Please highlight the selected stations on a station map (e.g. in Fig. 1).

RESPONSE: For the explosion signal we use all stations at components within the chosen range of epicentral distances, only excluding a few traces, based on lower signal-to-noise ratio. Signal amplitudes for the aftershock are significantly smaller than those of the main event. Since the signal-to-noise ratio of the aftershock is much lower that that of the main event, we decided to use only the best waveforms for each event individually.

CHANGES IN THE MANUSCRIPT: Figure 1 has been updated as suggested, also captions of figure 1 and 5 are updated in the manuscript.

2.3.3 COMMENT: page 7 figure 6: (a) It would be good arrange the Figure in two parts a) and b), a) showing the decomposition of the Moment tensor and b) showing the source type diagram. (same in Fig.8).
(b) I would find it very useful to explain roughly the Hudson-diagram, since it might be common sense for experts on moment tensor decomposition, however the paper is for a broader audience. For example all moment tensor solutions (beach balls) in the Hudson diagram represent double-couple solutions, while the best fit solution is mainly isotropic. Could you please comment on the representation and how one should read it?
(c) How was the ensemble of moment tensor solution retrieved? Do you use a statistical Monte-Carlo-type inversion? Give some more details and/or references in order to present reproducible results.

RESPONSE:
(a) The layout of Figure 6 and 8 actually fulfills the reviewer suggestion: the top part illustrates the

MT decomposition and the lower part the source type diagram. We improved figures caption to clarify this point.
(b) In the figure, the position of each beachball in the source type diagram describes the decomposition into isotropic, CLVD and DC. To provide more information we included beachballs, which describe the geometry of the DC term; however, in this case, DC terms are small for most MT solutions (they are far from the center of the diagram, which corresponds to pure DC solution). We improved the text and figure captions to clarify the figure and discussion for a broad audience.
(c) The optimization algorithm is described in Heimann et al. (2018), where the code is available (the reference has been now included); a dedicated manuscript on the methodology is stillin preparation. The method follows a sort of simulated annealing approach, first exploring the parameter space randomly, and later searching closer to best fitting solutions. Simultaneously a bootstrap approach is applied in order to investigate MT variability upon thedifferent weighting of different data. Figures 6 and 8 plot the ensemble of best solutions. We provide now more details in the manuscript with respect to the adopted method and procedure.

CHANGES IN THE MANUSCRIPT:
(a) Modified figure captions of figure 6 and added text on page 7 line 13.
(b) Text added on page 7 line 13.
(c) Text added on page 7 line 5.

2.3.4 COMMENT: page 7 figure 7: see comment 2.3.2.

RESPONSE: Please see reply to comment 2.3.2.

2.3.5 COMMENT: page 7 figure 8: see comment 2.3.3.

RESPONSE: Please see reply to comment 2.3.3.

2.4 Magnitude and Yield Estimation

2.4.1 COMMENT: You do not show any seismic section of the event. This is a pity. Here would be a good position to include one (maybe compare it to with waveforms of a previous test) and show the peak values that you are using to estimate mb. Show the 15 IMS stations you are using here on a map or give at least a reference, where one can find them.

RESPONSE: You are absolutely right, we should include some kind of seismic representation of the nuclear test (besides the traces shown in the MTI section). We will include example seismic recordings of the IMS primary seismic station GERES/PS19. For traceability, the 15 used stations for the magnitude estimation will be explicitly named in the text. An additional map could overload the article and add to much weight to this issue.

CHANGES IN THE MANUSCRIPT: page 7 subsection 2.4: We added the names of the seismic station used for the body wave magnitude estimation and added a figure showing seismic traces of the six DPRK tests recorded at the station GERES/PS19 in Germany. Furthermore we added more details to the text regarding the magnitude estimation.

2.4.2 COMMENT: page 8: *As no particular magnitude-yield relation has been approved so far for the North Korean test area, the latter relation by Bowers et al. (2001) is used in this study, as it supposedly most accurately represents the geological conditions at the test site.* Can you please comment on why the geological setting is supposed to be similar to Nova Zemlya? More important, is the North Korean test area known to consist of wet hard rock, rather than of dry unconsolidated rock? It changes the interpretation dramatically (by one order of magnitude). Give some references.

RESPONSE: Actually, we cannot provide proofed hints to associate the seismic coupling in Punggye-ri

rather to the conditions in Novaya Zemlya than to the conditions in Semipalatinsk. However, wet hard rock as general site condition can be stated. See references by Pabian and Coblentz.

CHANGES IN THE MANUSCRIPT: page 8 line 10: Changed/added text in the manuscript on page 8 line 10.

2.5 Influence of the Mt. Mantap Topography

2.5.1 COMMENT: The absolute transmitted energy is in all cases the same. A focusing/defocusing effect to certain slowness ranges is modeled. The conclusion is, that a focusing of the energy to small slownesses might result in an overestimation of the magnitude.
(a) For the discussion of this point I would ask the authors to be more quantitative. Give numbers: For which slowness range the energy is increased/decreased. Is it relevant only for teleseismic records or also for regional ones. Could a focusing to small slownesses also lead to an underestimation of the magnitude when using local/regional stations?
(b) Please discuss on the frequency ranges that are affected by the topography: For which frequency ranges the focusing effect is relevant? The lens (concave mirror) of the mountain has a range of approx. 2 km. For a P-wave velocity of 5.7 km/s wavelengths of the same dimension have a frequency of 2.85 Hz. Thus, I would expect, that the focusing is effective only for high frequencies (¿ 2.5 Hz). Will this still affect the magnitude estimation from teleseismic records?
(c) You show the topography effect in this chapter, however, you do not consider the topography in any of your analysis in the other chapters, especially for modeling the depth phases. Would the topography effect also effect the depth estimation by using pP phases? Please comment on that, since otherwise the paper appears to be incoherent.

RESPONSE:
(a) The focussing effect has only been investigated for a teleseismic slowness range. In figure 10 seismic energy is recorded in a rectangular box in a depth of 4 km beneath surface. The lateral extents of the box covers a slowness range for teleseismic P-phases from -9 to +9 s/degree. In our study local and regional phases have not been considered because yield is estimated using only teleseismic P-phases. Local and regional magnitude estimations are normally based on Lg-phases, these phases are not modeled in this study.
(b) In our simulations we model a broad frequency range using a point source with a delta shaped source time function. Under your assumptions for a P-wave velocity (5.7 km/s) and a lateral extent for the mountain (2 km), only waves with a frequecy above 2.85 Hz would be able to resolve the structure of the mountain. This holds true for tomographical studies for example. In the case of reflections at the surface, also waves with frequencies lower than 2.85 Hz will be affected. Therefore the focusing is effective also for lower frequencies, which are typically used in the estimation of teleseismic body wave magnitudes.
(c) We see no inconsistency between those two approaches, since the topography causes no change in differential travel times (see figure 10, bottom) but only influences the amplitudes of pP-phases. These amplitudes are not considered in the depth phase modeling approach. The influence of topography on moment tensor inversion is not studied in this paper. However we feel that topography might lead to a slight decrease of the volumetric part of the moment tensor. But this has to be investigated further in dedicated study dealing with a full wave propagation simulation on a regional scale.

CHANGES IN THE MANUSCRIPT:
(a) Added a sentence on page 8 line 31 to clarify the investigated slowness range.
(b) No changes in the manuscript.
(c) Added a sentence on page 9 line 12.

2.5.2 COMMENT: page 9 lines 6ff: *In general, this numerical modeling gives indications for: (1) Clear infrasonic signals, because surface reflections with higher amplitudes correspond to transmitted amplitudes with higher amplitudes yielding a transmission coefficient greater than 2 (see Section 3).*
(a) *Higher amplitudes* Higher than what?
(b) Where in section 3 are you taking about transmission coefficients?
(c) For me, it is not clear how you relate the pure elastic modeling to the elasto-acoustic transmission coefficient.

RESPONSE:
(a) Thank you for this comment, this sentence is a bit unclear. We rephrased the sentence for better understanding.
(b) You are correct, we are not talking about the transmission coefficient in the Infrasound section. We do not mention transmission coefficient in the rephrased sentence. See also comment 2.5.2a.
(c) The relation between elastic and acoustic energy has not been modeled in this study. Nevertheless it is well documented phenomena that infrasound is generated by earthquakes with a similar magenitude as the 2017 test. See for example Mutschlecner, 2005.

CHANGES IN THE MANUSCRIPT:
(a) Modified the sentence on page 9 line 6.
(b) See 2.5.2a.
(c) No changes in the manuscript.

3 Infrasound

3.1 COMMENT: page 9 line 23: *Figure 11a highlights the waveform beam of the Russian 4-element infrasound array I45RU (denoted as the co-located seismic station USRK in Figure 1a).*
(a) Please give here or in the next sentence the distance of I45RU to the test-site.
(b) It is surprising, that the It phase shows the strongest amplitudes. Is this in agreement with the modeling?

RESPONSE:
(a) We added the distance of around 400 km in the text.
(b) Yes, this is in good agreement with the corresponding modeling, we refer you to comment 3.3.

CHANGES IN THE MANUSCRIPT:
(a) page 9 line 21: added the distance of 401 km.
(b) see response to comment 3.3.

3.2 COMMENT: page 9 figure 11: The color code of the modeled ray travel-time is not chosen well to show differences in travel time of It and Is2.

RESPONSE: That is a valid comment, thank you. It is hard to visualize the difference as the propagation times for It and Is2 are very similar. As a compromise I added the exact traveltimes to the figure caption to highlight the similar traveltimes of the two phases.

CHANGES IN THE MANUSCRIPT: figure 11: Slight changes in the figure caption.

3.3 COMMENT: page 10 lines 11-16: *The signal attenuation indicates that only a small portion of signal energy is ducted in the stratosphere caused by partial reflections from gravity wave variations of the stratospheric mean background. This leads to higher attenuation in the stratospheric duct and thus stronger signal amplitudes in the thermospheric duct, which corresponds to the observed waveforms.* Please explain this point in a bit more detail. This is interesting. Why is the amplitude of It even larger than Is2?

RESPONSE: Parabolic equation modeling was performed (and is shown as the background color of figure 11c) to quantify the attenuation of the signal. The attenuation is 4.9 dB lower for the thermospheric duct compared to the stratospheric duct, resembling a factor of pressure amplitude increase of 1.8. Attenuations are derived and averaged from the PE modeling at the station distance of 401 km for a 2 km wide central section of the respective duct; total values of attenuation are -46.7 dB for the stratospheric duct and -41.8 dB for the thermospheric duct, both estimated with a signal frequency of 1 Hz. For 2 Hz, the values are -48.5 dB and -44.4 dB, the difference is 4.1 dB, equaling a factor of 1.6, accordingly. It is slightly less, but in the same order of magnitude, since thermospheric signals are more strongly attenuated at higher frequencies.

CHANGES IN THE MANUSCRIPT: page 10 lines 11-16: The resulting dB numbers and amplitude factors are added at page 10 lines 11-16. Furthermore the term *parabolic-equation modeling* is mentioned in the text.

3.4 COMMENT: page 10 lines 18-20: *Apart from the strong epicentral surface movement, infrasonic signatures were also identified from seismo-acoustic coupling and the assumed cavity collapse associated to the eight minute subsequent aftershock.* This is interesting. In 400km distance? Can you show these data? (maybe put it in the supplement).

RESPONSE: We added rather detailed supplementary information to this manuscript highlighting the early and late infrasound arrivals detected at I45RU and explaining their origins, as proposed.

CHANGES IN THE MANUSCRIPT: page 10 line 20: Added text to refer to the supplementary material.

4 Remote Sensing Studies

4.1 COMMENT: page 11 line 13-14: Figure 12 shows the surface deformation restricted to the test site area after the 2017 test for pixels with a coherence of greater than 0.25. → Figure 12 shows the surface deformation at the test site area during the 2017 test restricted to pixels with coherence values greater than 0.25.

RESPONSE: Changed as suggested.

CHANGES IN THE MANUSCRIPT: page 11 line 13-14: Changed the sentence as suggested by the reviewer.

4.2 COMMENT: figure 12:
(a) Displacement scale should have more numbers. (You only show ¿10 and ¡10). Please add at least a 0 and +/-5. (b) Please add the legend, explaining the colors of numbered circles, which is present in Fig 1b), to avoid misinterpretation of these colors with displacement values.

RESPONSE:
(a) Added more numbers to the legend in figure 12 (0cm, -5cm and 5cm).
(b) You are right, these colours are misleading. I removed the colors of the numbered circles to avoid misinterpretation with the displacement values.

CHANGES IN THE MANUSCRIPT: Slight changes to figure 12.

4.3 COMMENT: page 11 lines 18-20: *Due to the incidence (43°) and lock angle (ENE) of the sensors and the calculated slope and aspect angle (20° to 27° facing SW, 10° facing NE) based on Shuttle Radar Topography Mission data, 30 to 80 % of the vertical measured displacements in the area are detected.* 30-80% is a very wide range. I do not understand the statement. Please clarify.

RESPONSE: This sentence is hard to understand, thank you for the comment. We rephrased the sentence in the manuscript. Hope it is easier to understand now.

CHANGES IN THE MANUSCRIPT: Replaced the sentence
Due to the incidence (43°) and lock angle (ENE) of the sensors and the calculated slope and aspect angle (20 to 27° facing SW, 10° facing NE) based on Shuttle Radar Topography Mission data, 30 to 80 % of the vertical measured displacements in the area are detected. The recognition of the displacements is only possible in line of sight in the direction towards or away from the sensor
with the sentence
Due to the incidence and look angle of the sensor measured with respect to the ground and north direction, respectively, it is not possible to fully resolve the amount of the vertical surface displacement caused by the 2017 nuclear test. During data acquisition on August 29th and September 12th 2017 the sensor had an incidence angle of 43° and look angle facing East North East. These angles combined with the topography of Mt. Mantap result in the maximum mensurable percentage of vertical surface displacement. For the western flank of Mt. Mantap pointing towards the sensor with a slope of around 27° the percentage of resolvable surface discplacement is only around 30%, for the eastern flank pointing away from the sensor with a slope of around 10° the value of maximum menaurable surface displacement increases to around 80 %.

4.4 COMMENT: page 11 lines 20-27:
(a) I could not find the tunnel entrance on Fig 12 of Fig 1b. Please mark it in Figure 12.
(b) Please comment, why your processing of TerraSAR-X did not work here, while Wang et al was able to calculate the displacements.
(c) addtional → additional
(d) calcultes → calculates

RESPONSE:
(a) You are right the tunnel entrance is missing in figure 12. To avoid overloading of the figure I changed the passage in text from *tunnel entrance* to *main support area*. The main support area is shown in the figure 12 as well as in figure 1b.
(b) Wang used a different method to analyse the TerraSAR-X data set. The author used the method of amplitude tracking (also called pixel-offset-tracking or feature-tracking). This is a different method and is mainly used to investigate data sets with bad coherence values (for example glacier movements). Coherence values can be low for very strong ground movements (as for example in the case of the nuclear test). For the method used in this study coherence loss in the center of the test area was to high, and it was therefore not possible to calculate the ground displacements in the central area.
(c) Typo corrected.
(d) Typo corrected.

CHANGES IN THE MANUSCRIPT:
(a) page line 21: tunnel entrance → main support area.
(b) No changes in the manuscript.
(c) page 11 line 24: addtional → additional.
(d) page 11 line 25: calcultes → calculates.

4.5 COMMENT: page 11 lines 27-32: *To validate the displacement maps of the DInSAR analysis of the nuclear test, Pleiades data sets from August 26th and from September 8th 2017 were processed to reveal surface characteristics related to test (Figure 13). Change detection analysis show numerous landslides activated during the test and aftershocks.* How does the results validate each other? For the reader it is not clear how they are related. Please show the locations of the purple patches also in map view to make the results comparable.

RESPONSE: The temporal and spatial connection of the strong landslides (results obtained from the Pleiades data set) and the nuclear test allow the conclusion, that the landslides are caused by the test. We added a sentence in the text to underline this connection. Also the figure was changed according to your suggestions.

CHANGES IN THE MANUSCRIPT: Figure 13 is changed according to your suggestions. Also a sentence is added on page 11 line 29 to underline the relation between landslides and test/aftershock: *This relation is concluded by the strong temporal and spatial connection of the landslides to the test and aftershock origin time and epicenter locations.*

4.6 COMMENT: page 11 lines 32-33: *As a result of the processing of the ALOS-2 data, an area of around 3×4 km2 can be delineated, where surface movement rates range between -10 and 10 cm.* Is this result of relevance for the conclusions or discussion? Can you show these results? Where is this area located?

RESPONSE: This is just an observation of how large the effected surface area is. It simply underlines the strenght of the 2017 test in comparison to the former tests. I will add a sentence in the manuscript and also outline the area on the map.

CHANGES IN THE MANUSCRIPT: Added a sentence in text comparing the area of the 2017 event to the January 2016 test. Also modified figure 12 and caption of figure 12.

5 Radionuclide Monitoring and Atmospheric Transport Modeling

5.1 COMMENT: page 12: *During October three peaks containing five samples with 133 Xe activity concentrations between 0.5 and 1 mBq/m3 were measured at the station RN58, which went back to operation in between, atthe days indicated by the forward simulations.*
(a) Please describe the data that you want to explain by modeling at the begin of the section. Both data-sets with positive detections should be described, the one from South Korea that you want to disprove coming from the test site, as well as the one from RN58, that might be explained by a late release from the test site.
(b) What is the exact timing of the detections at RN58?
(c) Why did you choose October 4th and not any other day in October to run your simulations?

RESPONSE:
(a) The analysis of the raw radionuclide data is not within the scope of this study. The radioxenon concentrations measured in national capacity in South Korea (north-eastern stationary measurements) are taken from the cited press release. Please note that we don not "want to disprove" a suggested origin of the radioactive xenon isotopes, we just figured out that the overlay of the simulated source regions indicate another coincident source region than the test site. The xenon measurement data taken at RN58 are confidential according to the CTBT framework. We used the collection times of samples for which an elevated concentration of 133Xe was reported to the State Signatories for the timing of our backward simulations.
(b) The backward calculations for RN58 were made for 12 hour air samples from 00:00-12:00 (UTC) on 5th, 6th, 19th, 26th and 27th of October 2017.
(c) The forward dispersion modelling starting October 4th is complementary to the backward simulation from RN58 on October 5th. It is just one example for the fairly direct atmospheric connection from the test site to Ussurysk. Similar simulations are available for the other dates with elevated 133Xe at RN58.

CHANGES IN THE MANUSCRIPT:
(a) page 12 line 29: text changed for better understanding.

(b) page 12 line 29: Added sample times in the text.
(c) page 12 line 27: Text adjusted for clarification.

6 Discussion

6.1 COMMENT: page 13 line 14: *The depth phase modeling of the P-waveform was performed at 2.5 Hz and found a centroid depth between 400 m and 800 m, which is within the expected resolution of about half the wavelength.* What do you want to state here? Seismograms have been filtered between 0.5 and 2.5 Hz (See caption Fig. 3). You do not show the spectral content of the signal. Clearly 2.5 Hz is only the upper limit. If 400 m is half a wavelength, lambda=800 and c=lambda*f = 800*2.5=2 km/s for the upper limit and c=800*0.5=400m/s for the lower limit. This is too low for P-waves velocities, so I do not get the point here.

RESPONSE: As mentioned in the paper, we used CRUST 2.0 profiles at the source and receiver side for waveform modelling. According to the regional model at the source side, the expected P-wave wavelength is aprrox. 1000 m, which indicates that the depth is still resolvable. This point is made more clearly in the revised manuscript.

CHANGES IN THE MANUSCRIPT: Revised the text on page 13 line 12-16 for clarification.

6.2 COMMENT: page 14 line 2ff:
(a) main event around eight minutes later a large → main event, around eight minutes later, a large.
(b) that this is event → that this event.
(c) event is at least a partial → event is caused by at least a partial.

RESPONSE:
(a) Changed as suggested.
(b) Typo corrected, thanks for the hint.
(c) Changed as suggested.

CHANGES IN THE MANUSCRIPT:
(a) page 14 line 2: main event around eight minutes later a large → main event, around eight minutes later, a large.
(b) page 14 line 3: that this is event → that this event.
(c) page 14 line 3: event is at least a partial → event is caused by at least a partial.

7 Conclusions

7.1 COMMENT: page 15 line 22 : *Explosive character of the September 3rd 2017 North Korean event is confirmed by cross correlation and MTI analysis.* How does cross correlation confirm the explosive character of the event?

RESPONSE: Earlier events where identified as nuclear explosions. High correlations between the 2017 event and earlier events might lead to the conclusion that the 2017 event is also a nuclear explosion. But you are right, it is a little bit measleading and not clear. I removed the term *cross correlation* from the manuscript.

CHANGES IN THE MANUSCRIPT: page 15 line 22: removed the words *cross correlation.*

7.2 COMMENT: page 15 line 26ff: *The estimated yield of the nuclear device is certainly smaller than the largest documented yield ever achieved by a boosted fission device and is therefore still compatible with a fission only device.* On the other hand: would it also be compatible with a small fusion bomb?

RESPONSE: Yes. We cannot exclude that fusion was involved. It is beyond our expertise to speculate if it would be technically even more difficult to limit the yield of a thermonuclear device to a few hundreds kt TNT than reaching the megaton range (as other states did with their first tests of hydrogen bombs).

7.3 COMMENT: page 15 line 27-28: *Strong surface deformations (+-10 cm) are observed in an area of 3x4 km2. Furthermore multiple landslides as well as a number of aftershocks were observed in the aftermath of the test.* This is the observation. What is here the conclusion? → either skip this point or add a conclusion to the observation.

RESPONSE: Please see response to comment 4.4. I will add some text to the conclusion to underline the enormous power of the 2017 test.

CHANGES IN THE MANUSCRIPT: page 15 line 28: Added text underlinig the explosive power of the 2017 test.

7.4 COMMENT: page 16 line 3-4: No immediate measurements of radionuclides related to the test in September were observable, but later occurrences of radionuclides are consistent with a delayed leakage from the test site in October. − > Due to the non-operating radionuclide station RN38, no immediate measurements of radionuclides related to the test in September were observable. However, later occurrences of radionuclides are consistent with a delayed leakage from the test site in October.

RESPONSE: It is not clear if there would have been radionuclide measurements in September with an operational station RN58. If we write *Due to the non-operating...*, it would imply that there would have been measurements. We suggest to leave the sentence as it is at the moment to avoid misunderstandings.

7.5 COMMENT: page 16 line 5: The test site might be strongly stressed and shattered and might be rendered useless for further test activities. − > The test site might have been strongly stressed and shattered and thus rendered useless for further test activities.

RESPONSE: Changed as suggested.

CHANGES IN THE MANUSCRIPT: page 16 line 5: The test site might be strongly stressed and shattered and might be rendered useless for further test activities. − > The test site might have been strongly stressed and shattered and thus rendered useless for further test activities.

Responses to referee 2 (Anonymous)

Manuscript SE-2018-102

A Multi-Technology Analysis of the 2017 North Korean Nuclear Test

Peter Gaebler, Lars Ceranna, Nima Nooshiri, Andreas Barth, Simone Cesca, Michaela Frei, Ilona Grünberg, Gernot Hartmann, Karl Koch, Christoph Pilger, J. Ole Ross, and Torsten Dahm

Dear reviewer,

we want to thank you for taking the interest and time to deliver this very helpful and constructive review of our work. We studied your comments and made changes and corrections to the manuscript where necessary. We hope our changes and and corrections are sufficient to make our article suitable for publication soon. Your comments and suggestions certainly helped to improve quality and clarity of the paper.

Respones to your comments are given in the following pages. We first respond to your general comments and then respond to your specific comments as given in your annotated pdf version of the manuscript. Changes made in the manuscript related to your comments are given in blue color, changes by the authors after rereading the manuscript are given in grey color. Changes related to the comments by the first reviewer Felix Schneider are given in green color. Page and line numbers refer to the originally submitted manuscript.

Thank you again,
best regards

Peter Gaebler and co-authors

General Comments

G1 COMMENT: The document as such appear to be rather a catalog of result that a multi-technology analysis, which could be achieved through establishing the objective of such an approach and adding discussion and transition between methods and technologies.

RESPONSE: Thank you for this comment. Indeed the results are obtained within the disciplines of seismology, infrasound monitoring, remote sensing and atmospheric transport modeling. But we want to stress, that there are cross-links where the methods and technologies complement each other and lead to a consistent multi-technology picture of the event analysis. For example this is true for the hypocenter estimation of the event, where remote sensing and seismological methods are combined to achieve aboslute information about the epicenter and the depth of the event. This is described on page 4 lines 20-25. Also for example we use data from different DRPK events to infer the epicenter location. As the area of surfacedisplacement of the 2017 event is of great extent and no definite epicenter location can be derived from the 2017 test, data from the January 2016 event is used, which showed a clear a distinct maximum of surface displacement (see page 15 line 9-12). To clarify cross-connections between

the methods and technologies we adapted the manuscript text at some positions.

CHANGES IN THE MANUSCRIPT:
(a) page 9 line 14: Added following transition sentence: *For a shallow event in that magnitude range it is expected to record infrasound signals in distances of up to hundreds of kilometers (Mutschlecner and Whitaker, 2005).*
(b) page 11 line 32. Added following transition sentence: *The strong surface deformations at the surface observed for the 2017 test might lead to pathways and the subsequent release of radionuclides, especially gaseous radionulcides such as 133Xe, from the test site. Potential measurements of radionuclides are discussed in the following Section 5.*
(c) page 15 line 9: Changed sentence to underline the cross-link between seismology and remote sensing technologies.

G2 COMMENT: Noteworthy, the link between the different seismological methods should be emphasized and discussed, and in particular the differences in estimations.

RESPONSE: Also here the different seismological methods can be interpreted as stand-alone results. But for example depth is estimated using multiple different methods (double difference method, moment tensor analysis and depth phase method). The different estimations and also the resulting differences are discussed on page 13 lines 11-16. Furthermore we for example discuss the influence of topography on the estimation of the body wave magnitude and therefore also the influence on the estimated yield (page 20 lines 20-33). Of course in the field of seismology, many more interdependencies can be imagined and have to be further elaborated, for example the possibility to estimate yield reversely over collapse-strength/cavity size. Further interdependency analysis is beyond the scope of this study.

G3 COMMENT: The fusion of results between technologies also needs to be further introduced and discussed.

RESPONSE: To our understanding, *Data Fusion* applies to the first phase when grouping data of different IMS technologies which potentially belong to the same critical event. Our multi-technology analysis covers more aspects of an Expert Technical Analysis, where a critical event is investigated in depth with additional methodologies. We added text concerning data fusion in the introduction of the manuscript.

CHANGES IN THE MANUSCRIPT: page 2 line 16: Added text concerning data fusion. *To assess the connection between radionuclide detections and potential source events atmospheric tranport modeling (ATM) is applied. Grouping data from different IMS technologies that is attributed to the same critical event is refered to as data fusion.*

G4 COMMENT: Questions that the manuscript should answer are:
(a) what are the author trying to achieve by having a multi-technology approach?
(b) and in the end, did they achieve it and if not, what was the reason? (technology/resolution limitations, insufficient knowledge at the interface between technologies...?)

RESPONSE:
(A) By applying a multi technology analysis we try to give an overall characterization of the explosion and its consequences, ideally connected with a reliable yield estimate and a statement on the type of the device. All these points are covered in the manuscript.
(b) Yes, the evidence from this study would be compelling enough to state a treaty violation in the context of the CTBT. Beyond this, neither the yield estimate nor the radionuclide evidence was sufficient for full characterization of the nuclear device which would be of further interest for intelligence quarters and policy makers. The main reasons are the high uncertainties in yield estimation and the largely contained radionuclides. A potential On-Site Inspection could achieve additional evidence. We added

text in the conclusions to underline the achievement of the multi-technology analysis.

CHANGES IN THE MANUSCRIPT: Added text on page 16 line 6: *The combination of the results from the different technologies and methods yields a reliable estimation of hypocenter, magnitude, explosive energy, source mechanism as well as an indication for delayed leakage of ^{133}Xe from the test site. The cross-links between the different results complement each other in a consistent manner.*

Specific Comments

0 Abstract

0.1 COMMENT: page 1 line 16: ehance → enhance.

RESPONSE: Typo corrected.

CHANGES IN THE MANUSCRIPT: page 1 line 16: ehance → enhance.

1 Introduction

1.1 COMMENT: page 2 line 9: remove *or in space.* This is covered by the Outer Space Treaty, not the CTBT.

RESPONSE: Thank you for this comment, you are correct. Space is not covered by the CTBT.

CHANGES IN THE MANUSCRIPT: page 2 line 9: removed the words *or in space.*

1.2 COMMENT: page 2 line 11: are still missing ratification → have still not ratified.

RESPONSE: Changed as suggested.

CHANGES IN THE MANUSCRIPT: page 2 line 11: are still missing ratification → have still not ratified.

1.3 COMMENT: page 2 line 22: even definite → even though definite.

RESPONSE: Changed as suggested.

CHANGES IN THE MANUSCRIPT: page 2 line 22: Added the word *though.*

1.4 COMMENT: page 3 line 2: *successful test of a fusion bomb* Please provide a reference.

RESPONSE: We now provide a reference to a press release by the Korean Central News Agency regarding the successful test of H-bomb for ICBM.

CHANGES IN THE MANUSCRIPT: page 3 line 2: Added reference KCNA2017.

1.5 COMMENT: page 3 line 8: Typo. As there is not → as there is no.

RESPONSE: Thank you for pointing that out, the typo is corrected.

CHANGES IN THE MANUSCRIPT: page 3 line 8: As there is not → As there is no.

1.6 COMMENT: page 3 line 17: in teleseismic → at teleseismic.

RESPONSE: Changed as suggested.

CHANGES IN THE MANUSCRIPT: page 3 line 17: in teleseismic → at teleseismic.

1.7 COMMENT: page 3 line 19: Additionall, → Additionally.

RESPONSE: Typo corrected.

CHANGES IN THE MANUSCRIPT: page 3 line 19: Additionall, → Additionally.

1.8 COMMENT: page 3 line 19-20: *is estimated by 2D-waveform modeling to estimate.* Repetition of estimate.

RESPONSE: Thank you for this comment, we avoided the repetition by using the term *assess.*

CHANGES IN THE MANUSCRIPT: page 3 line 20: estimate → assess.

1.9 COMMENT: page 3 line 21: Typo: test site, The → test site. The

RESPONSE: Typo corrected.

CHANGES IN THE MANUSCRIPT: page 3 line 21: changed comma to point.

2 Seismological Investigations

2.2 Estimation of Hypocenter Depth and Seismic Moment

2.2.1 COMMENT: page 4 line 30-32: *However, such a depth phase approach needs high-frequency waveforms above 1 Hz to resolve the onset of the depth phase, and may be difficult from single stations recordings if the signal to noise ratio (SNR) is poor at teleseimsic distances.* Incomplete sentence.

RESPONSE: You are right, thanks for the comment. There was something missing. We added *to be performed* to the text to form a complete sentence.

CHANGES IN THE MANUSCRIPT: page 4 line 31: Added the word *to be performed* to form a complete sentence.

2.2.2 COMMENT: page 5 figure 3: Issue with the figure.

RESPONSE: Issue should be resolved, sorry for the inconvinience.

2.2.3 COMMENT: page 6 line 11: *from (Bassin et al, 2000)* parenthesis to fix.

RESPONSE: Thank you for the comment, the brackets are correct, but the term CRUST2.0 was missing in front of the brackers. Corrected in the text now.

CHANGES IN THE MANUSCRIPT: page 6 line 11: Added the term *CRUST 2.0* in front of the citation of Bassin et al, 2000.

2.2.4 COMMENT: page 6 line 20: *(compare Dahm er al., 2007)* Compare with - can you be more specific.

RESPONSE: This is a misplaced reference. I removed the term *compare Dahm et al., 2007* from the manuscript.

CHANGES IN THE MANUSCRIPT: page 6 line 20: removed the citation of Dahm et al., 2007.

2.2.5 COMMENT: page 6 line 20: Interesting → Of interest.

RESPONSE: Changed as suggested.

CHANGES IN THE MANUSCRIPT: page 6 line 20: Interesting → Of interest.

2.2.6 COMMENT: page 23 figure 3: Figure should be redone/corrected, it is incomplete.

RESPONSE: See comment 2.2.2.

2.3 Moment Tensor Inversion of the Test and the Main Aftershock

2.3.1 COMMENT: page 7 figure 5: Difficult to read on paper version - author should improve quality/resolution/size.

RESPONSE: Due to the format of the EGU latex template the figure is smaller than it will be in the final form. I would suggest to wait for the final editing of the manuscript and then redo the figure if required.

2.3.2 COMMENT: page 7 line 20 : *still show a good SNR* Define what is a good SNR, can there be a qualitative metric?

RESPONSE: Thank you for this valid comment. Good in this context means, that the signal strength is sufficient to be used for MTI analysis. I modified parts of the sentence for clarification.

CHANGES IN THE MANUSCRIPT: Modified text on page 7 line 20.

2.3.3 COMMENT: page 7 line 25 : page 25 figure 5: Ok on the PDF, but difficult to read on printout.

RESPONSE: Please see comment 2.3.1.

2.5 Influence of the Mt. Mantap Topography

2.5.1 COMMENT: page 8 line 19: in 0.8 km depth → at 0.8 km depth.

RESPONSE: Changed as suggested.

CHANGES IN THE MANUSCRIPT: page 8 line 19: in 0.8 km depth → at 0.8 km depth.

3 Infrasound

3.1 COMMENT: page 9 line 28: *Infrasonic forerunner* Is it forerunner or could it explained by the ground coupling effect, since 1) an area could be radiating rather than a single point or 2) the ground-coupling location is located closer to the station, which suggest longer seismic propagation and shorter infrasound path.

RESPONSE: The signal recorded after about 1350 seconds shaping a third PMCC signal group is suspected to be a separate detection following another propagation path, since its trace velocity and back-azimuth directions differ from those of the Is2 detection. It was estimated to be an acoustic forerunner, since the observed celerities still have adequate acoustic values indicative of an early infrasound arrival. Nevertheless it is also possible that the sound is related to the infrasound radiation of an extended epicentral (or near-epicentral) area instead of an epicentral point source (reviewers proposal 1)). We added this possibility to the manuscript text. Reviewers proposal 2) is an option that is covered in larger detail by a study on seismo-acoustic coupling following the underground nuclear test. It is added to the manuscript as a supplement following the comments and requests of the first reviewer. Also see the response to comment 2 regarding this supplementary information.

CHANGES IN THE MANUSCRIPT: page 9 line 27-29: We added *to infrasound radiation from an extended (near-)epicentral source region* in the text.

3.2 COMMENT: page 10 line 7-8: *Figure 11c models the propagation from the test site epicenter to the station I45RU using parabolic equation and ray-tracingmethods for the attenuation of signal amplitude and the connection of source and receiver by eigenrays.* Walker et al for Tohoku earthquake and Le Pichon et al for 2005 Chilean earthquakes came up with representation for ground coupling regions that could be of value here.

RESPONSE: Investigations on ground coupling regions (where seismic wave signatures are in certain surface regions converted into infrasound then propagating to the station) were already requested to be discussed in further detail by the first reviewers. We added a supplement to the manuscript to present results from this study. Ground coupling regions and corresponding detections are described there. We take into account the proposed references and added them to the supplement.

3.3 COMMENT: page 10 line 16: in 400 km → at 400 km.

RESPONSE: Changed in the manuscript as suggested.

CHANGES IN THE MANUSCRIPT: page 10 line 16: in 400 km → at 400 km.

3.4 COMMENT: page 31 figure 11: see comment in 3.1 about the forerunner.

RESPONSE: We want to refer you to our response to comment 3.1.

4 Remote Sensing Studies

4.1 COMMENT: page 11 line 25: Typo: calcultes → calculates.

RESPONSE: Typo corrected.

CHANGES IN THE MANUSCRIPT: page 11 line 25: calcultes → calculates.

4.2 COMMENT: page 11 line 29: related to test → related to the underground test.

RESPONSE: Changed as suggested.

CHANGES IN THE MANUSCRIPT: page 11 line 29: related to test → related to the underground test.

5 Radionuclide Monitoring and Atmospheric Transport Modeling

5.1 COMMENT: page 12 lines 12-15: *The IMS station RN58 (Ussurysk, Russia) would have been affected, but was not operational at that time. Station RN38 (Takasaki, Japan) would have been missed by the plume from the potential release from the test site which is typical for the season. Stations further downwind, for example in Northern America, would have required a larger release for activity concentrations to exceed the detection threshold.* Sentences should be rewritten if possible less conditional and more specific.

RESPONSE: We made slight adjustements in the text. We feel that the sentence is clear now. Please comment further if you do not agree with our formulation.

CHANGES IN THE MANUSCRIPT: page 12 line 11: Text slightly changed to make it more specific and less conditional.

5.2 COMMENT: page 12 line 23: *Nyongbyon County.* Incomplete. For clarity, it should be homogenized with the figure showing the nuclear facility.

RESPONSE: We used the term Yongbyon Research Center in the text now for clarification. The research complex is shown in the figure. I hope this solves the problem.

CHANGES IN THE MANUSCRIPT: page 12 line 23: Slight adjustments to the text.

5.3 COMMENT: page 13 line 1: *delayed small releases.* Please explain and clarify the 1) delay and 2) "small".

RESPONSE: *Delayed:* The potenital releases under discussion took place within 30 to 50 days after the test. *Small:* Small refers to required source term in the order of roughly 10^{11} Bq. This number is given in the prior sentence on page 12 line 35.

A Multi-Technology Analysis of the 2017 North Korean Nuclear Test

Peter Gaebler[1], Lars Ceranna[1], Nima Nooshiri[2], Andreas Barth[3], Simone Cesca[2], Michaela Frei[1], Ilona Grünberg[1], Gernot Hartmann[1], Karl Koch[1], Christoph Pilger[1], J. Ole Ross[1], and Torsten Dahm[2]

[1] BGR, Federal Institute for Geosciences and Natural Resources, Hannover, Germany
[2] GFZ, German Research Centre for Geosciences, Potsdam, Germany
[3] KIT, Karlsruhe Institute of Technology, Karlsruhe, Germany

Correspondence: Peter Gaebler (peter.gaebler@bgr.de), Stilleweg 2, 30655 Hannover, Germany

Abstract. On September 3rd 2017 official channels of the Democratic People's Republic of Korea announced the successful test of a thermonuclear device. Only seconds to minutes after the alleged nuclear explosion at the Punggye-ri nuclear test site in the mountainous region in the country's northeast at 03:30:02 (UTC) hundreds of seismic stations distributed all around the globe picked up strong and distinct signals associated with an explosion. Different seismological agencies reported body wave magnitudes of well above 6.0, consequently estimating the explosive yield of the device in the order of hundreds of kilotons TNT equivalent. The 2017 event can therefore be assessed being multiple times larger in energy than the two preceding North Korean events in January and September 2016.

This study provides a multi-technology analysis of the 2017 North Korean event and its aftermath using a wide array of geophysical methods. Seismological investigations locate the event within the test site at a depth of approximately ~~0.8~~0.6 km below surface. The radiation and generation of P- and S-wave energy in the source region is significantly influenced by the topography of the Mt. Mantap massif. Inversions for the full moment tensor of the main event reveal a dominant isotropic component accompanied by significant amounts of double couple and compensated linear vector dipole terms, confirming the explosive character of the event. Analysis of the source mechanism of an aftershock that occurred around eight minutes after the test in the direct vicinity suggest a cavity collapse. Measurements at seismic stations of the International Monitoring System result in a body wave magnitude of 6.2, which translates to an yield estimate of around 400 kilotons TNT equivalent. The explosive yield is possibly overestimated, since topography and depth phases both tend to enhance the peak amplitudes of teleseismic P-waves. Interferometric Synthetic-Aperture-Radar analysis using data from the ALOS-2 satellite reveal strong surface deformations in the epicenter region. Additional multispectral optical data from the Pleiades satellite show clear landslide activity at the test site. The strong surface deformations generated large acoustic pressure peaks, which were observed as infrasound signals with distinctive waveforms even in distances of ~~400 km~~401 km. In the aftermath of the 2017 event atmospheric traces of the fission product ^{133}Xe have been detected at various locations in the wider region. While for ^{133}Xe measurements in September 2017 the Punggye-ri test site is disfavored as source by means of atmospheric transport modeling, detections in October 2017 at the International Monitoring System station RN58 in Russia indicate a potential delayed leakage of ^{133}Xe at the test site from the 2017 North Korean nuclear test.

1 Introduction

The Comprehensive Nuclear-Test-Ban Treaty (CTBT) and its associated entity, the Preparatory Commission for the CTBT organization (CTBTO), are dedicated to monitoring and banning nuclear explosions worldwide – underground, in water ~~,~~or in the atmosphere ~~or in space~~. ~~It~~The CTBT was opened for signature in 1996 but will only enter into force after the 44 nuclear technology holders (states listed in the Annex 2 of the CTBT) will have signed and ratified the treaty. At the time of this study, eight Annex 2 states ~~are still missing ratification~~have still not ratified the treaty, including North Korea. To detect, locate and characterize nuclear explosions an International Monitoring System (IMS) was established by the CTBTO as part of a verification regime. The IMS features four different approaches for the monitoring of potential nuclear explosions. Three methods (seismology, infrasound and hydroacoustics) are attributed to waveform technologies and have the purpose of detecting, localizing and identifying suspicious events with an explosive source mechanism. The fourth approach features the monitoring of particulate radionuclides and noble gases in the atmosphere and potentially provides the unambiguous evidence of the nuclear character of an explosion. To assess the connection between radionuclide detections and potential source events atmospheric transport modeling (ATM) is applied. Grouping data from different IMS technologies, that is attributed to the same critical event, is refered to as data fusion. For further information on the CTBT, the IMS, and the German National Data Center the reader is referred to Pilger et al. (2017) or CTBTO (2018).

Since the first known nuclear test, carried out by the Unites States in 1945, more than 2000 confirmed nuclear explosion tests were conducted by China, France, Great Britain, India, North Korea, Pakistan, Russia and the United States. It is generally accepted that all six past explosions in North Korea between 2006 and 2017 have been nuclear underground tests. This study therefore refers to the events in North Korea as nuclear tests, even though definite proof might be missing. North Korea is the only country breaking the de facto moratorium on nuclear tests. For detailed information on the first five North Korean tests see for example Hartmann et al. (2017).

All past North Korean nuclear tests were conducted at the Punggye-ri test site in the vicinity of Mt. Mantap in the northeastern part of the country. Following the geologic description of the test site area provided by Coblentz and Pabian (2015) and Pabian and Coblentz (2017), Mt. Mantap is made out of two distinct geologic formations. The core of the mountain consists of igneous basement rock of either diorite or granite, while the top is capped by a thin layer of basaltic lava flows. The basement crystalline rock and the top layer of Mt. Mantap are separated by a nearly horizontal sequence of volcanic deposits with a thickness of around 200 m. The origin of these deposits is suspected to be volcanic ash from Mt. Paektu, a volcano located around 100 km northeast. Due to their loose consolidation, the volcanic deposits are softer then the basement rock or the basaltic layer and are

therefore more susceptible to erosion. Furthermore, the volcanic layer is more exposed to erosional scars and landslides due to its steeper slope. The erosion of the volcanic layer can cause the overlaying basalt cap to break off at the scarp, which is visible in larger piles below the volcanic layer where the slope of the mountain slightly decreases.

The official channels of North Korea announced the 2017 event as a successful test of a fusion bomb (Korean Central News Agency, 2017). This would be a major step in the nuclear program of North Korea. From a scientific point, therefore, the depth of the event, its strength in terms of radiated high- and low-frequency seismic energy, the contribution of possible faulting or slope instability processes, the near surface damage in the test area as well as the proof wether fission products are detected as atmospheric tracers are key questions to be answered. These questions are approached by an integrated study based on different seismological (Section 2), infrasound (Section 3), remote sensing (Section 4), radionuclide monitoring (Section 5), and modeling techniques which complement each other. As there is not easy concept to verify and characterize nuclear explosions, especially in a country where direct observations are difficult to assess, this study demonstrates and emphasizes the strength of an integrated multi-technology approach.

In this context, new methodical approaches are introduced to improve the depth estimate from teleseismic observations and to quantify uncertainties in the non-isotropic source component. Radionuclide monitoring demonstrates the importance of atmospheric transport modelling (ATM)to avoid over-interpretation of variations in ^{133}Xe concentrations. The seismological study retrieves an independent absolute location based on a combination between seismological and remote sensing data. The relative location between the six North Korean nuclear tests is obtained by means of waveform cross correlation time lag data. The event depth is estimated for the first time by a joint inversion of source time function (STF) and depth phase waveform modelingwaveform composition of direct and depth phases observed at small aperture, high-frequency arrays inat teleseimsic distances. A full waveform moment tensor inversion (MTI) is applied and compared to results of previous explosions onin North Korea. The source time overshoot and peak amplitude is compared to traditional body wave magnitudes (m_b) estimates. Additionally, the effect of topography on peak amplitudes is estimated by 2D-waveform modeling to estimateassess the possible range of explosive yield. Infrasound observations and modeling is used to understand the earth-atmosphere coupling and the propagation of infrasound from the North Korean test site.. The analysis of satellite based remote sensing data is important to improve the absolute location of shallow sources as well as to quantify the secondary mass movement effects at the surface. Radionuclide monitoring demonstrates the importance of ATM to avoid over-interpretation of variations in ^{133}Xe concentrations. While radionuclide monitoring provides the only direct evidence of nuclear explosions, it is demonstrated by careful modeling how difficult it is to interpret such data and that early claims of causal anomalies have possibly been over-interpreted.

2 Seismological Investigations

2.1 Epicenter Location

The localization in the Reviewed Event Bulletin (REB) of the CTBTO International Data Center (IDC) uses 125 seismic stations of the IMS and results in an epicenter of 41.321°N and 129.035°E with an error ellipse area of 110 km^2. This relatively

high error is generated by the fact that only eight IMS stations are located at distances from 400 km up to 2100 km (see Figure 1a).

Figure 1

However, the incorporation of 25 additional seismic stations in regional distances cannot significantly improve the absolute location estimate, as the closest station MDJ is still 372 km away from the test site. Due to these large source-receiver distances a further improvement of the absolute location accuracy is limited. Nevertheless, relative location methods can be applied for a high precision localization of the events (Zhang and Wen, 2013; Zhao et al., 2014, 2016; Gibbons et al., 2017). In this study a relative location procedure based on the cross-correlation of seismograms from 33 regional seismic stations for the six North Korean tests is applied. Seismograms for the past North Korean events significantly vary between the stations, due to propagation paths from source to the surrounding stations at different distances and azimuths. However, the correlation of the seismograms of the six events for each individual station shows a good coherence between the corresponding signals with the Pn-phase being the most pronounced arrival in the waveforms. These signals are correlated for each individual station, which has recorded at least two North Korean nuclear tests. The cross-correlation between each pair of events is performed using normalization to 1.0 for the auto-correlation of each signal at zero lag. Maximum correlation values of 0.7 to 0.99 are obtained for stations up to 1100 km distance for the four tests in the years 2009, 2013 and 2016. Due to significant differences in explosive yield, and therefore different source time durations, the 2006 and 2017 test are slightly less correlated with the other tests. See Figure 2 for the complete results of the cross-correlation analysis.

Figure 2

~~Time lags of the maximum cross-correlation values are used to determine precise travel time differences with an accuracy in the order of the sampling rate.~~ The estimation of time lags turned out to be reliable, when the maximum cross-correlation values exceeded a threshold of 0.4. With this constraint, a subset of 165 event pairs for 19 stations was selected, for which precise travel time differences with an accuracy in the order of the used sampling rate of 0.025 s could be determined. Pn-phase onset times of all tests are aligned to the onset at the closest station MDJ and fixed as relative start time for the estimation of the correlation time lags at the other stations. A double difference method (e.g. Waldhauser and Ellsworth, 2000) is applied to cross correlation time lags and results suggest that the last five events are located within a radius of 400 m, while the 2006 test is located around 2 km further to the east (see Figure 1b). The relative locations of the six tests can be associated to absolute coordinates as soon as the geographical coordinates of one of the tests are known. The geographic, absolute location of the January 2016 nuclear explosion is fixed by means of radar interferometry data to the location of the maximum surface deformation observed after the test (Hartmann et al., 2017; Wei, 2017). The absolute epicenter location of the 2017 test from relative location procedures is consequently determined to be 41.3007°N, 129.0728°E (Figure 1b).

2.2 Estimation of Hypocenter Depth and Seismic Moment

The source depth is needed to estimate the explosion process and strength of the seismic source. However, constraining the depth of a shallow source is difficult from regional and teleseismic data without a close ~~epicentral station above~~station within

a focal depth's distance from the source. The ~~analysis of the time lag of near-source,~~ modeling of the wavelet consisting of a surface-reflected P-phase~~s~~, so-called depth phase~~s~~, and STF can potentially help in such a case~~.~~, ~~because they only depend on the depth and the P-wave velocity in layer above the source. However, such a depth phase approach~~ Such a wavelet modeling approach resembles the inverted and time-shifted STF and needs high-frequency waveforms above 1 Hz to resolve the onset of the depth phase, and may be difficult to be performed from single station~~s~~ recordings if the signal to noise ratio (SNR) is poor at teleseimsic distances. An approach uncommon for nuclear test studies is used, which was established for the analysis of induced seismicity, where waveform beams are calculated at several small-aperture, short-period arrays to enhance the SNR (Figure 3a).

Figure 3

The beam waveforms represent a superposition of direct and reflected waves. The depth of the explosion is estimated by comparing observed and synthetic beam waveforms (Figure 3d), which are calculated for the best moment tensor solution described in Subsection 2.3, a common STF and varying depths. The source time is represented as a composition of multiple basis functions with unknown weighting coefficients, which are estimated in a least squares inversion with smoothing constraint (Figure 4). If $u(t)$ is the seismogram (beam) at the array with coordinates $\mathbf{r}_r$ and from a seismic source with coordinates $\mathbf{r}_s$, the P-wave train (i.e. P- plus pP- plus sP-phase) at time t is represented by

$$u(t) \quad = \quad \{M_{jk} G_{j,k}(\mathbf{r}_s, \mathbf{r}_r, t)\} * m(t)\,, \tag{1}$$

where $*$ is a time convolution and where the summation convention is applied. $G_{j,k}$ are the spatial derivatives of the Green's function, where the comma before index $_{,k}$ indicates a spatial derivative with respect to x_k. It is assumed that all moment tensor components M_{jk} have the same time dependency, which is described as normalized ~~STF~~moment function $m(t)$ with $m(t \to \infty) = 1$. The ~~waveform of far-field displacement pulses are~~displacement in the far-field is controlled by the time derivative of $m(t)$, which is declared as moment rate function $\dot{m}(t)$. ~~The P-wave from an earthquake $\dot{m}(t)$ has a~~ This explains that the far-field body-wave pulses from earthquakes are single-sided pulses (Dahm and Krüger, 2014). Since only the far-field wavefield is considered, the Green's functions in (1) are replaced by far-field Green's functions $G^{(ff)}$, and $m(t)$ is replaced by $\dot{m}(t)$. The inversion is ~~setup~~set up for $\dot{m}(t)$ using a set of N time-shifted triangular basis functions $h_l(t)$ (Figure 4):

$$\dot{m}(t) = \sum_{l=1}^{N} \beta_l h_l(t)\,, \tag{2}$$

where β_l is a weighting factor and each $h_l(t)$ satisfies $\int h_l(t)dt = 1$.

Figure 4

Hence, equation (1) is written as

$$u(t) \quad = \quad \left\{ M_{jk} G^{(ff)}_{j,k}(t) \right\} * \begin{bmatrix} h_1(t) & h_2(t) & \dots & h_N(t) \end{bmatrix} \cdot \begin{bmatrix} \beta_1 \\ \beta_2 \\ \vdots \\ \beta_N \end{bmatrix}. \tag{3}$$

The convolution in (3) can be ~~equated and~~written in discrete form, leading to an over-determined matrix system for unknown weighting factors to be solved in a least squares sense using the L_2-norm (Dahm and Krüger, 2014). If more than one array is available, the equations are added to the coefficient matrix to realize a joint inversion. Additionally, the STF inversion is stabilized by using a regularization with a roughness matrix. The STF is inverted for every single trial depth. The length of the STF is constrained to 1.5 s, where 0.5 s are considered before the arrival of the P-wave. It should be noted that, with shorter length of STF, the details of the STF with a complex structure are difficult to resolve. On the other hand, with longer length of the STF, i.e. larger number of basis functions, the fitted curve oscillates wildly and gives a very poor representation of the model, which is known as over-fitting. The length of the STF mentioned before was chosen to reach a compromise, after examining the residual misfit in total signal variance computed for different lengths of source time function. In order to compensate travel-time residuals occurring along the mantle ray zero-lag Green's functions are correlated with P-wave beams at every array, and the travel-time corrections are considered before the inversion. The source depth itself is estimated using a grid search approach, where the depth of the point source Green's functions is sampled from 0 to ~~1000 m~~1500 m in 100 m steps. For every depth solution the residuals are estimated and stored for final evaluation.

Green's functions are calculated using the code QSEIS (Wang, 1999), where source and station specific crustal models can be considered. AK135 (Kennett et al., 1995) is used for the mantle, while different crustal ~~models~~profiles for source and station regions are taken from CRUST 2.0 (Bassin et al., 2000). Intrinsic attenuation for P-waves is set to 5000, since otherwise high frequencies are damped out at teleseismic distances. The sampling frequency is 20 Hz. The grid search depth phase modeling has been applied previously to different cases of induced seismicity (Dahm et al., 2007) and the 2016 nuclear explosion (Cesca et al., 2017), but the simultaneous STF inversion is implemented for the first time in this study.

The full waveforms of beams, their peak heights and peak distances are well fitted in a joint inversion of four arrays. The best fits are obtained at depths between 400 to 800 m (Figure 3b). However, it should be noted that the depth value obtained from the inversion procedure might be overestimated due to the use of an unperturbed velocity model. Perturbations in the velocity model for example through potential fracturing above the explosion, which would substantially reduce~~d~~ P-wave velocity, were neglected. If the source of the synthetic beams is placed deeper or shallower, the duration and appearance of the P-, pP- and sP-pulses changes and residuals increase. ~~Interesting~~Of interest are the retrieved moment rate and moment function, which show a clear double pulse and overshoot, respectively (Figure 3c). Such an overshoot is not expected for the rupture process of tectonic earthquakes, where the moment rate and moment functions of the P-wave are single sided pulses and monotonously increasing functions, respectively. ~~but commonly observed for nuclear explosions.~~ For nuclear explosions, however, this feature is commonly observed. ~~It~~This can be explained by at least a partial collapse of the explosion cavity immediately after the explosion. In this case, the final moment is only 23 % of the peak moment in Figure 3c. The inversion of long-period waves led to a seismic moment M_0 of 2.33×10^{17} Nm, representing the time after the overshoot. The peak seismic moment is thus estimated in the range of $M_{0,peak}\approx1.02\times10^{18}$ Nm. The associated low- and high-frequency moment magnitudes (M_W) are M_W=5.55 and $M_W^{(\mathrm{peak})}$=5.97, respectively, and can explain the large difference between the long period M_W and the high-frequency m_b estimates which emerged during the magnitude estimation described in Subsection 2.4.

2.3 Moment Tensor Inversion of the Test and the Main Aftershock

Seismic signals of the 2017 North Korean test show a great similarity to those generated by the previous four nuclear tests conducted in 2009, 2013, and 2016. Especially long period waveforms with periods above 10 s recorded at regional distances show a high waveform similarity and a substantially increased amplitude, revealing a very similar radiation pattern of all events and a larger moment release for the 2017 nuclear test. In recent years, MTIs have been performed for nuclear tests in North Korea, including those carried out in 2009, 2013 and 2016 (Ford et al., 2010; Barth, 2014; Vavryčuk and Kim, 2014; Cesca et al., 2017; Hartmann et al., 2017). All MTI were performed by fitting low-frequency full waveform seismic data at regional distances, either in the time or in the frequency domain. The majority of these solutions revealed a significant positive isotropic component. For the 2013 nuclear test an extraordinary high double couple (DC) component was found, indicating differences in containment or near source damaging effects (Barth, 2014; Vavryčuk and Kim, 2014). For the 2017 test the seismic moment tensor is inverted by fitting the low frequency amplitude spectra (epicentral distances up to 1200 km) and full displacement waveforms (epicentral distances up to 600 km) in the frequency range from 0.02 to 0.04 Hz following the approach by Cesca et al. (2013, 2017). For the moment tensor optimization the Grond algorithm (Heimann et al., 2018) is used, which searches the parameter space by random search first and later by an increasingly denser search around the best solutions. The algorithm finally resolves the full moment tensor components, the centroid location and centroid time, and also provides information on model uncertainties and source parameters trade-offs. Full waveforms and their spectra are calculated assuming a layered crustal model proposed by Ford et al. (2010). Example full waveform displacement and amplitude spectra fits are shown in Figure 5.

Figure 5

The moment tensor solution for the 2017 test shows a dominant positive isotropic part of 60 %, 16 % positive compensated linear vector dipole (CLVD), and 24 % of DC. The best solution, found at a depth of around 2 km, has a scalar moment of 2.33×10^{17} Nm, equivalent to a M_W of 5.55. The centroid depth is poorly resolved and good waveform fits are found for very shallow sources down to 2.5 km. This result confirms the very shallow depth of 400-800 m accurately resolved by the analysis of depth phases in Subsection 2.2. The moment tensor optimization resolves a broad ensemble of well fitting moment tensor solutions. ~~(Figure 6), either dominated by a positive isotropic component, a negative vertical CLVD, or a combination of both, what has been attributed to trade-offs among moment tensor components for very shallow sources (Cesca et al., 2017; Cesca and Heimann, 2017).~~They are plotted using a source type diagram in Figure 6 and are characterized by strong deviations from a pure DC model (mapping in the center of the diagram), a typical model for tectonic earthquakes. Instead, acceptable solutions are either dominated by a positive isotropic component (positive values of the y-axis in the plot), a negative vertical CLVD (positive values of the x-axis), or a combination of both. The variability among these type of solutions has been attributed to trade-offs among moment tensor components for very shallow sources (Cesca et al., 2017; Cesca and Heimann, 2017). This range of moment tensor solutions includes alternative moment tensor configurations as proposed for previous nuclear explosions in North Korea (e.g. Barth, 2014).

Figure 6

In the aftermath of the nuclear test, a seismic event took place in its direct vicinity around eight minutes later. The estimated scalar moment and M_W are 1.88×10^{16} Nm and 4.81, respectively, and thus the scalar moment is only $\sim$8 % of the one of the nuclear test. The waveforms of the aftershock still show a ~~good~~sufficient SNR~~, and the signal strength is sufficient~~ to perform a MTI. Waveform displacement and amplitude spectra fits of the MTI are shown in Figure 7.

Figure 7

The inversion is based on spectral and waveform fits at stations located within 1000 km epicentral distance, filtered between 0.02 and 0.04 Hz. The calculated depth of the aftershock is similar to the depth of the explosion. The best MTI solution suggests a dominant implosive source component (65 %), negative CLVD (29 %) and a DC component of 6 %. This source mechanism is compatible with a shallow collapse source or might hint to some kind of break-in process. An ensemble of well fitting moment tensor solutions for this inversion is shown in Figure 8.

Figure 8

2.4 Magnitude and Yield Estimation

The determination of m_b is the prerequisite for a reliable estimation of the yield of a nuclear explosion. In order to obtain comparable results for the past six North Korean events, m_b is calculated from waveform peak values measured at always the same 15 IMS seismic stations that recorded all six events. ~~These stations cover the entire azimuthal range and are located at distances between 3700 and 9000 km from the Punggye-ri test site.~~ These stations (MKAR, INK, FINES, WRA, YKA, ASAR, AKASG, HFS, NOA, VRAC, GERES, STKA, DAVOX, NVAR, PDAR) cover the entire azimuthal range with a maximum gap of 121 degrees and are located at distances between 3700 and 9000 km from the Punggye-ri test site. Exemplarily, the seismic signals at the German primary seismic station GERES are shown in Figure 9. The high similarity between the six nuclear explosions is standing out due to the short and simple P-wave train. The recordings differ only in the amplitudes. The resultant single station magnitude for GERES was used together with the corresponding magnitudes of the other 14 involved stations to obtain reliable and comparable average magnitudes.

Figure 9

For the 2017 test a m_b of 6.2 is calculated, compared to m_b values of 4.1 to 5.3 for the five preceding tests. In general it is not possible to state one single relation between magnitude and yield, as this relation depends on various factors, such as the geological setting at the source site, the efficiency of wave propagation from source to receiver, the depth of the explosion and the coupling of the source to the underground. A number of empirical formulas of the type $m_b = A + B\log(Y)$, with Y being seismic yield in kilotons TNT equivalent and A and B being constants depending on the aforementioned factors, have been developed to relate yield and m_b. These relations have been successfully used for yield calibration for example at the Nevada test site (Murphy, 1981), in Kazakhstan (Ringdal et al., 1992) or in Nova Zemlya (Bowers et al., 2001). As no

particular magnitude-yield relation has been approved so far for the North Korean test area, the latter relation by Bowers et al. (2001) is used in this study., as it supposedly most accurately represents the geological conditions at the test site. The North Korean nuclear explosions were mainly conducted beneath the Mt. Mantap complex, consisting of stratified volcanics covering a basement of granite and diorite. In general, wet hard rock can be taken into account for these geological conditions, when the yield is estimated on base of the seismic magnitude. Under these assumptions a yield of around 400 kilotons TNT equivalent is estimated for the September 2017 test, clearly illustrating a steady increase of explosive strength of the nuclear tests (see Figure 10).

Figure 10

2.5 Influence of the Mt. Mantap Topography

Two-dimensional synthetic wave-field simulations are used to study the influence of topography of the Mt. Mantap complex on the propagation of P- and S-wave energy emitted by a point-like explosion source. A Chebyshev pseudospectral method (e.g. Tessmer et al., 1992) is used for modeling the elastic wave-fields on a Cartesian 820×512 grid for an 8 km×5 km box in x- and z-direction, respectively. No variation of medium properties is assumed in the y-direction. Figure 11 shows the model configurations as well as the wave propagation for an explosion source inat 0.6 km depth below surface (see Subsection 2.2).

Figure 11

The source time function is taken from Glasstone and Dolan (1977, Chapter 6), where the source duration is 0.15 s. The wave-field V is separated in divergence ($|\nabla \cdot V|$) and curl ($|\nabla \times V|$) reflecting the P- and SV-energy, respectively. Moreover, the wave propagation is considered for one model without and two models with topography; whereas the topography is considered for a west-east profile along 41.3°N crossing the Mt. Mantap massif (see Figure 1b). The velocity model is chosen such that it reflects the petrology of the local geology as described by Coblentz and Pabian (2015). However, strong lateral variations as thrust or normal faulting in the uppermost layers are not taken into account due to reasons of numerical stability. Instead lateral variations, which are based on an exponential perturbation with a correlation length of 100 m, are considered with differences in density, P- and S-wave velocities of ±3 %. Merely, the last model accounts for erosion of the uppermost basaltic and volcanic layers as well as an almost vertical dyke reflecting the transition between the granodiorites and the granite from west to east. Nevertheless, computing the P-divergence and SV-curl in a rectangular box shows large differences in the downward propagating wave-fields, where strong increases for both pP- and pS-wave amplitudes can be observed. The position and the lateral extent of this box covers a slowness range from -9 $s/°$ to +9 $s/°$, which are typical slowness values for teleseismic P-waves. For a source under Mt. Mantap surface reflections are increased in their amplitudes by a factor of ∼1.5 due to topography. Wave energy is focused due to the shape of the mountain, especially from the easterly flank with a change in altitude of approximately 600 m (see Figure 1b). Topography is the crucial factor, the difference between the two simulations with and without a realistic geologic setting (see Figure 11, middle and right panels) is negligible. Further simulations for sources shallower and deeper as the reference value of a depth of 0.6 km below surface provided similar pictures; whereas for sources shallower than 0.5 km and deeper than 1.7 km, respectively, energy focusing is less pronounced with amplifications in am-

plitude of 1.3 and less. Although only a two-dimensional model is considered, such simulations are also valid for the three-dimensional nature because Mt. Mantap exhibits a high symmetry. In general, this numerical modeling gives indications for: ~~(1) Clear infrasonic signals, because surface reflections with higher amplitudes correspond to transmitted amplitudes with higher amplitudes yielding a transmission coefficient greater than 2 (see Section 3).~~ (1) Generation of clear infrasonic signals (see Section 3), because topography (slope of Mt. Mantap) increases the amount of radiated acoustic energy in sub-horizontal direction, which is the usual propagation path for infrasound (compare Figure 12). (2) A reduced value of the isotropic part obtained by MTI because a larger amount of S-wave energy is generated in the source region due to topography effects above the source (see Subsection 2.3). (3) An overestimation of the yield of the explosion, because P- and pP-phases are considered as a single onset in teleseismic distances and in the investigated frequency range for shallow sources, leading to an increase in maximum P-wave amplitude of approximately 1.3 and hence in m_b of around 0.1, respectively. (4) No effect on differential travel times between P- and pP-phases due to topography, therefore no effect on hypocenter depth estimation using depth phase modeling (see Section 2.2).

3 Infrasound Observations

For a shallow event in the given magnitude range it is expected to record infrasound signals in distances of up to hundreds of kilometers (Mutschlecner and Whitaker, 2005). Infrasound is sub-audible sound below the human hearing threshold of 16 Hz and is the dedicated monitoring technology of the CTBTO for remotely detecting atmospheric explosions. Furthermore, infrasound can be used in civil and scientific applications such as the monitoring of volcanoes, meteoroids, ocean swell and various other natural and anthropogenic activities (see Le Pichon et al. (2010) for a comprehensive overview). Infrasound signals are alsogenerated by strong underground or underwater sources when the generated waves couple into the atmosphere. The North Korean tests between 2006 and 2016 were investigated and registered by various infrasound arrays (Che et al., 2014; Assink et al., 2016; Park et al., 2018; Koch and Pilger, 2018). Detections of the 2013 test by the IMS stations I30JP in Japan and I45RU in Russia were part of the REB and thus confirmed the underground nuclear test as source of infrasound waves. For the 2017 test, the station I45RU, located in a distance of 401 km from the test site, detected infrasound signatures from the nuclear test (see also Assink et al., 2018). Clear waveforms undoubtedly associated to the nuclear test were recorded and were again part of the REB. Figure 12a highlights the waveform beam of the Russian 4-element infrasound array I45RU (denoted as the co-located seismic station USRK in Figure 1a).

Figure 12

Coherent waveform signals can be observed and associated to infrasound propagation from the nuclear test site arriving at I45RU after travel times of 1450 s and 1520 s, corresponding to celerities of 290 m/s and 270 m/s, respectively. Preceding waveform activity at around 1350 s (315 m/s) can either be associated to infrasound radiation from an extended (near-)epicentral source region or the fast acoustic phase of an infrasonic forerunner (Evers and Haak, 2007). These values are in the pure acoustic range and indicate stratospheric ducting (Is_2 with two reflections and Is_{1f} with one elongated reflection, turning heights of 40 to 55 km) and thermospheric ducting (It, turning heights above 100 km) (Drob et al., 2003). It is

the first time that an underground nuclear test is strong enough to generate distinct and far-reaching pressure signatures that were clearly recorded at a remote IMS infrasound station after propagation through the thermosphere above 100 km altitude. The corresponding Progressive Multi-Channel Correlation (PMCC, Cansi, 1995) analysis of the signal content in terms of time variation, frequency content and back-azimuth direction is illustrated in Figure 12b. The PMCC method draws rectangular time-frequency-windows wherever correlated signal energy in three or more array elements is present. Color-coded back azimuths between 210° and 225° (southwest) point towards the Punggye-ri nuclear test site with a true back-azimuth of 218°. Effects from cross winds (west to north-west, strongest in the stratosphere) lead to the fact that the observed back-azimuths are some degrees lower, especially within the stratospheric duct. The PMCC signatures with broadband frequency content from 0.2 to 4 Hz can thus clearly be associated to the 2017 DPRK nuclear test.

Figure 12c models the propagation from the test site epicenter to the station I45RU using parabolic equation and ray-tracing methods for the attenuation of signal amplitude and the connection of source and receiver by eigenrays. A combination of European Centre for Medium-Range Weather Forecasts (ECMWF) analysis data and climatological profiles is implemented for temperature and wind model backgrounds including gravity wave perturbations (see Koch and Pilger (2018) for further details on the methods and the atmospheric profiles used). The eigenrays show that the stratospheric phases are about 170 s and 70 s faster than the thermospheric phase (caused by a higher effective sound speed in the stratosphere and the longer wave path for the thermospheric phase). The signal attenuation, as obtained from parabolic-equation modeling, indicates that only a small portion of signal energy is ducted in the stratosphere caused by partial reflections from gravity wave variations of the stratospheric mean background. This leads to about 4 to 5 dB higher attenuation in the stratospheric duct and thus stronger signal amplitudes in the thermospheric duct by a factor of 1.6 to 1.8, which corresponds to the observed waveforms. The presented infrasound signals clearly observed even ~~in~~at ~~400 km~~401 km distance and with disadvantageous propagation conditions are indicative for a strong surface movement in the epicentral area (see Section 4) of the underground test generating large acoustic pressure peaks as argued in Subsection 2.5. Apart from the strong epicentral surface movement, infrasonic signatures were also identified from seismo-acoustic coupling and the assumed cavity collapse associated to the eight minute subsequent aftershock (see the supplement to this manuscript for further information).

4 Remote Sensing Studies

To visualize and characterize the surface imprint of the 2017 test radar data from the ALOS-2 satellite (Suzuki et al., 2009) and multispectral optical data from the Pleiades satellite (Gleyzes et al., 2012) are investigated. Data from the ALOS-2 satellite in the L-band (1257.5 MHz frequency, 3 m resolution) are analyzed by Interferometric Synthetic Aperture Radar (InSAR) to investigate surface deformations (subsidence and uplift) correlated with the 2017 test and its aftershocks. The method of change detection analysis based on the Normalized Differential Vegetation Index (NDVI) is applied. Spaceborn InSAR has been used to detect surface displacements of the Earth's surface since more than 20 years (Massonnet et al., 1993) and has reached maturity in recent years (Adam et al., 2009), nowadays allowing for the detection of surface displacements with a precision in the order of a few millimeters. Repeat pass interferometry is based on the registered interferometric phase per

ground cell (pixel) and is related to the distance differences between the scatterer and the SAR sensor between two acquisitions separated in time. The interferometric phase measured as moduli 2π is thus ambiguous. To solve this ambiguity, frequency estimations using unwrapping techniques are calculated. The Earth's curvature, topography and atmospheric effects influence the interferometric phase in addition to surface displacements. These phase contributions have to be estimated and subtracted to correctly estimate the surface displacement (Kampes, 2006). In addition, the backscattered electromagnetic signal between the acquisitions times needs to be correlated or coherent. Decorrelation can be caused by (1) temporal (large separation between the acquisitions in time), (2) geometrical (large perpendicular baseline) and (3) scattering effects (incoherent movement of scattering elements within the pixel, Gatelli et al., 1994).

Differential InSAR (DInSAR) processing was adjusted to the test site target area regarding above mentioned constraints. As the investigated area is located in a mountainous region, DInSAR processing is challenging due to factors such as limited visibility for SAR acquisition geometry, tropospheric phase contributions and/or snow cover and vegetation causing temporal phase decorrelations. DInSAR processing encompasses following steps: co-registration, filtering, unwrapping and the discussion of coherence. Coherence serves as a measure of the quality in ~~DInSar~~DInSAR studies, with coherence values ranging from 0.0 to 1.0, with 1.0 suggesting a perfect interferogram with no noise. For the analysis of the surface displacement due to the 2017 test, data from August 29th and from September 12th 2017 is used, data coherence between these two times has a mean value of 0.6 for the investigated area. For areas that show surface deformation the coherence values range from 0.2 to 0.8.

Figure 13 shows the surface deformation at the test site during the 2017 test restricted ~~to the test site area after the 2017 test~~ to pixels with ~~a~~ coherence values ~~of~~ greater than 0.25.

Figure 13

In the central part of the Mt. Mantap massive, coherence values dropped significantly below 0.25 due to very strong ground deformations (see also Wang et al., 2018). The recognition of the displacements is only possible in line of sight in the direction towards or away from the sensor. ~~Due to the incidence (43°) and look angle (ENE) of the sensors and the calculated slope and aspect angle (20 to 27° facing SW, 10° facing NE) based on Shuttle Radar Topography Mission data, 30 to 80 % of the vertical measured displacements in the area are detected. The recognition of the displacements is only possible in line of sight in the direction towards or away from the sensor.~~ Due to the incidence and look angle of the sensor measured with respect to the ground and north direction, respectively, it is not possible to fully resolve the amount of the vertical surface displacement caused by the 2017 nuclear test. During data acquisition on August 29th and September 12th 2017 the sensor had an incidence angle of 43° and look angle facing East North East. These angles combined with the topography of Mt. Mantap result in the maximum measurable percentage of vertical surface displacement. For the western flank of Mt. Mantap pointing towards the sensor with a slope of around 27° the percentage of resolvable surface discplacement is only around 30%, for the eastern flank pointing away from the sensor with a slope of around 10° the value of maximum measurable surface displacement increases to around 80 %. The resulting map of resolvable displacements clearly shows an area of subsidence of up to 10 cm around 3 km north of the ~~tunnel entrance~~main support area (compare Figure 1b), and an area with clear uplift of up to 10 cm west of the Mt. Mantap peak. DInSAR processing of C-Band Sentinel data and TerraSAR-X data for the 2017 test did not reveal acceptable

quality measures regarding coherence in the central part of Mt. Mantap, whereas for the tests in 2016 Sentinel data did show excellent results (Hartmann et al., 2017; Wei, 2017). A study by Wang et al. (2018) shows ~~addtional~~ additional results based on amplitude images from TerraSAR-X data and ~~calcultes~~calculates 0.5 m subsidence in the centre and 3.5 m of horizontal displacement. This strong spatial and temporal coincidence of the displacement areas to the nuclear test site suggests a high correlation with the underground test. To validate the displacement maps of the DInSAR analysis of the nuclear test, Pleiades data sets from August 26th and from September 8th 2017 were processed to reveal surface characteristics related to the underground test (Figure 14). This relation is concluded by the strong temporal and spatial connection of the landslides to the test and aftershock origin time and epicenter locations.

Figure 14

Change detection analysis show numerous landslides activated during the test and aftershocks. As a result of the processing of the ALOS-2 data, an area of around 3×4 km^2 can be delineated, where surface movement rates range between -10 and 10 cm. For comparison, the area of the January 2016 North Korea nuclear test, which showed comparable surface movement rates, was in therange of 1.5×1.5 km^2 (Hartmann et al., 2017). This large difference clearly underlines the enormous power the 2017 nuclear test. The strong surface deformations at the surface observed for the 2017 test might lead topathways and the subsequent release of radionuclides, especially gaseous radionulcides such as ^{133}Xe, from the test site. Potential measurements of radionuclides are discussed in the following Section 5.

5 Radionuclide Monitoring and Atmospheric Transport Modeling

Measurements of radioactive fission products released into the atmosphere even at far distances can deliver the definite proof of the nuclear character of an explosion. To assess the consistency between measurements and potential source locations the method of ATM is applied (Becker et al., 2007; Ross et al., 2017). For the ATM analysis of potential detections of radionuclides the Lagrangian Particle Dispersion Model HYSPLIT (National Oceanic and Atmospheric Administration – Air Resources Laboratory, Stein et al., 2015) is used. The ATM is operated with meteorological data from the US National Centers for Environmental Prediction (NCEP). For the prediction of potentially affected radionuclide measurement stations, HYSPLIT is operated in forward mode with hypothetical releases. For the assessment of the potential source region of detected radioisotopes the model runs in backward mode. Dispersion simulations of a potential immediate release after the explosion on September 3rd 2017 show prevailing wind directions to the north east (Figure 15a).

Figure 15

According to the forward simulations, ~~T~~the IMS station RN58 (Ussurysk, Russia) would have been affected, but was not operational at that time. Station RN38 (Takasaki, Japan) would have been missed by the plume from the potential release from the test site which is typical for the wind patterns of the season. Stations further downwind, for example in Northern America, would have required a larger release for activity concentrations to exceed the detection threshold.

The South Korean Nuclear Safety and Security Commission issued a press release on September 13th 2017 with results of

national efforts to detect radioactive Xe isotopes after the test. The statement *'Considering the timing and location of sampling and air currents, the NSSC could conclude that the air currents from the North Punggye-ri area has been mixed to the sample and the Xe-133 detected from this air sampling is relevant to the 6th nuclear test of DPRK'* (Nuclear Safety and Security Commission, 2017) was interpreted by the media as source attribution. Backward simulations for the samples collected at the northeastern stationary measurement system at Geojin were performed using 500000 model particles per sample and 0.5° GDAS (Global Data Assimilation System) meteorological data. Additive overlay of the source regions of seven stationary 12-hour samples with elevated ^{133}Xe from September 7th to 10th 2017 points to the ~~Nyongbyon County~~region~~, and area~~ where the Yongbyon North Korean Scientific Research Center is located, as likely coincident source (Figure 15b), whereas the test site can be disregarded as common source for the seven samples. This contradicts the suggestions in the media that the detected ^{133}Xe originated from the test explosion.

~~Forward simulations from the test site show that the station RN58 would have been affected by hypothetical releases in October repeatedly.~~Continued forward simulations for hypothetical releases from the test site show that the station RN58 would have been affected by the plumes repeatedly during October. Figure 15c shows as an example the dispersion after 36 h of a hypothetical ten hour release on October 4th 2017 using HYSPLIT with 0.25° GFS (Global Forecast System) data and 1 million particles released. ~~During October three peaks containing five samples with ^{133}Xe activity concentrations between 0.5 and 1 mBq/m^3 were measured at the station RN58, which went back to operation in between, at the days indicated by the forward simulations.~~ In fact, the station RN58 went back to operation in between and three peaks of elevated ^{133}Xe activity concentration were measured on the days indicated by routine forward simulations from the testsite (October 5th, 19th, and 26th). Those peaks consist of five samples with ^{133}Xe activity concentrations between 0.5 and 1 mBq/m^3. Backward ATM results also indicate a high sensitivity of these five samples to being released from the test site. Figure 15d shows the overlap of the corresponding retroplumes at time of maximum sensitivity to the test site. A leakage in the order of 10^{11} Bq ^{133}Xe would have been sufficient to explain the detections at station RN58. Although the measurements and the ATM are consistent with delayed small releases from the test site in October, they cannot be unambiguously attributed to the North Korean test explosion.

6 Discussion

A combination of seismological analysis using a double-difference method and remote sensing technologies results in an epicenter location of the 2017 test of 41.3007°N, 129.0728°E, clearly placing the event inside the North Korean nuclear test site, in which all previous tests have been conducted. The epicenter location is confirmed by results from (Wang et al., 2018), who estimated an epicenter location of 41.300°N, 129.078°E ± 50 m, which places the two epicenter solutions only ∼400 to 500 m apart. On May 24th 2018 North Korea invited international media to witness the demolition of the Punggye-ri test site. During a demonstration North Korean officials presented a map showing the relative locations of the six nuclear tests (CNN, 2018). Allthough the correctness of the information provided by the North Korean government cannot be verified, comparisons indicate that the assumed locations fit the results from the independent relative location method reasonably well.

Two independent methods showed that the 2017 North Korea event was very shallow. The full waveform moment tensor inversion indicates a centroid depth in the range of about 2 km, but has a relatively poor resolution because of the long wavelength of low-pass filtered data. The depth phase modeling of the P-waveform was performed at 2.5 Hz and found a centroid depth between 400 ~~m~~and 800 m. According to the crustal profile at the source side, the expected P-wave wavelength is ~1000 m, which ~~is within the expected resolution of about half the wavelength~~ indicates that the source depth is still resolved. This is supposedly the best absolute centroid depth estimate possible from seismological data far from the source. Depth estimations in this study are comparable to results from Wang et al. (2018). The authors used numerical models to minimize the misfit between predicted and observed surface displacements and specified a depth of 450 $\pm$ 100 m.

The explosive character of the 2017 event is confirmed by MTI analysis, which indicates a dominant isotropic source part of around 60 %. These results are supported by studies by Liu et al. (2018) and Han et al. (2017), who also revealed a dominant positive isotropic source part. Under the assumption of the magnitude-yield relation following Bowers et al. (2001) the estimated m_b of 6.2 (see Subsection 2.4) for the event results in a yield of 400 kilotons TNT equivalent. This value is assumed to be an upper limit, as following reasons might lead to a yield overestimation: (1) Topography at the test site (see Subsection 2.5) strongly influences the radiation of seismic energy from the source. This results in higher amplitudes of the pP-phase. As the hypocenter location is very shallow, P- and pP-phases from the event arrive nearly simultaneously at distant receivers and superimpose at frequencies relevant for the estimation of m_b. This superimposition leads to an increase of approximately 1.3 in P-wave amplitude in the far-field and consequently to an increase in m_b of around 0.1. (2) Furthermore in the standard calculations of m_b (Gutenberg, 1945a, b; Bormann, 2012), distant-dependent correction curves, which are valid for a DC source, are applied. Gaebler and Ceranna (2017) state, that the use of correction terms for a shallow explosion source can lead to an overestimation of m_b of around 0.2. Taking both these effects into account, the originally estimated value for m_B of 6.2 had to be considered as an upper limit estimate and has to be corrected by a factor of up to 0.3. This correction leads to a lower estimate for m_B of 5.9, similar to $M_W^{(\text{peak})}$ that is estimated from the source time function, which translates to an estimated yield of around 160 kilotons TNT equivalent. Therefore indications are strong that yield might be overestimated, not only for the 2017 explosion, but also for all five previous North Korean nuclear tests.

Following the main event, around eight minutes later, a large aftershock of local magnitude m_L 4.1 was detected. MTI analysis of this event shows a clear negative isotropic part which leads to the conclusion that this ~~is~~event is caused by at least a partial collapse of the cavity formed by the main explosion. These findings are again supported Liu et al. (2018) and Han et al. (2017), who also find a clear negative isotropic source part for the aftershock. According to Liu et al. (2018), the aftershock can qualitatively be interpreted as a rapid destruction of an explosion-generated cracked rock chimney due to cavity collapse. Following this strong aftershock, nine more earthquakes with local magnitudes m_L ranging from 2.5 up to 3.2 were detected by the Korean Meterological Agency (Korean Meterological Agency, 2018) in the region (41.2 to 41.4°N, 129.0 to 129.2°E) until April 2018. Aftershocks in such magnitude range and quantity were not observed from the five previous tests from 2006 to 2016, but are not unusual for nuclear explosions of that size (Boucher et al., 1969).

In the aftermath of the 2017 event measurable surface activity was detected in the region of the Punggye-ri test site. Remote sensing results suggest a distinct pattern of uplift (up to 10 cm) in the western part of the Mt. Mantap massif and subsidence

(up to -10 cm) in the eastern part. The geological interpretation by Coblentz and Pabian (2015) and Pabian and Coblentz (2017) shows a north-south trend of various geological units ranging from carbonates, diorites, granites and gneises in contact to a younger basalt (layered volcanics) at Mt. Mantap. Furthermore, the structural pattern in the region suggests a north-south trending system of faults up to the main tunnel entrances, with a part of the fault system branching out to the north-west. Considering this geological background the deformation pattern can be interpreted as a (partial) uplift of the basement rocks in the western part. Eventually this is structurally controlled by the north-south trending reverse faults together with the unconformable capping of stratified volcanic sequences. This interpretation is confirmed by multispectral optical data from the Pleiades satellite which shows that the layered tuffs are strongly affected by intensive landslide activities.

Overall, accounting for all these activities (surface deformations, the collapse event, aftershocks, landslides) it can be argued, that the internal structure beneath Mt. Mantap might be strongly stressed and shattered due to the last six tests and might be rendered useless for further test explosions (see also Wang et al., 2018).

Despite these strong activities and the enormous release of seismic energy from the event no immediate release of radionuclides was measured by the IMS. This is a strong indication that no direct pathways from the cavity to the surface for the propagation of radionuclides were created during the test and the subsequent collapse-type aftershock. Only a few days after the 2017 event South Korea announced national measurements of ^{133}Xe and proposed a connection of these observations to the test. However, backward ATM calculations performed in the context of this study disfavor the Punggye-ri test site as possible origin for ^{133}Xe but rather point to the Yongbyon nuclear complex as a most likely coincident source region instead in September. Nevertheless, in October 2017 three peaks of ^{133}Xe were detected at the IMS station RN58 in Ussurysk, Russia. Forward as well as backward ATM show directly connecting dispersion conditions and indicate the North Korean test site as a likely source for the ^{133}Xe detections. Nevertheless, other regional sources cannot be excluded and it was not possible to definitely identify the presence of ^{131m}Xe in the RN58 samples, which – in the correct isotropic ratio – would have increased the evidence of a nuclear explosion source (Kalinowski et al., 2010), as for example shown for the 2013 North Korean nuclear explosion by Ringbom et al. (2014). According to calculations of concentration and sensitivity, a release at the test site in the order of a few 10^{11} Bq would have been sufficient to cause and explain the detections at station RN58. This is also quantitatively consistent as the required source term ranges well below the remaining fission inventory even after six to ten halflifes of ^{133}Xe (5.2 days) and a small leakage through mountain cracks. However, a direct number of the fission inventory is hard to estimate as the fission yield depends not only on the explosive yield but also on the type of nuclear device. Within the available data it is not possible to determine if nuclear fusion was involved in the process. The largest yield ever achieved by a boosted fission device was 720 kT TNT equivalent of the british *Orange Herald* in 1957. For this explosion an amount of 118 kg ^{235}U was mounted (Arnold and Pyne, 2001). The explosive yield in this study of between 160 and 400 kT TNT equivalent is therefore still fully compatible with a fission only device.

DInSAR results show a large area of strong displacement in the case of the 2017 test and it is not possible to demark a definite surface location of the test epicenter from these measurements. However retrieving a ground truth from DInSar measurements from the January 2016 test, which showed a clear and distinct maximum of surface displacement, can help to provide an absolute epicenter location of the 2017 test. By combining remote sensing and relative locations methods only the epicenter

of the event can be estimated. A third method (depth phase modeling) is required for the complete estimation of the 2017 test hypocenter. This method is further able to provide an explanation for the large difference in m_b and M_W, which has not been observed in this order for the previous tests. Furthermore while for previous weaker tests radionuclide measurements were able to prove the nuclear character of the explosions (Ross et al., 2017), radionuclide measurements alone in September 2017 could have been misleading in regards to the source area. This examples clearly demonstrate that an integrated multi-technology and multi-methodology approach is essential for a reliable and comprehensive identification and characterization of a potential nuclear test.

7 Conclusions

Overall, the following main conclusions can be deduced from this study:

- Explosive character of the September 3rd 2017 North Korean event is confirmed by ~~cross correlation and~~MTI analysis.
- Yield of the event is estimated to be around 400 kt TNT equivalent with indications that this value should be considered as an upper limit and might be as low as 160 kt TNT equivalent. This overestimation can be explained by the enhancement of peak amplitudes of teleseismic P-waves due to topography and depth phase effects.
- The estimated yield of the nuclear device is certainly smaller than the largest documented yield ever achieved by a boosted fission device and is therefore still compatible with a fission only device.
- Strong surface deformations ($\pm$10 cm) are observed in an area of 3$\times$4 km^2. Comparisons of affected surface area to the January 2016 test underline the enormous power the 2017 nuclear test. Furthermore multiple landslides as well as a number of aftershocks were observed in the aftermath of the test.
- The aftershock directly following the nuclear explosion has a similar depth as the test and can be characterized as a collapse of the cavity created by the test.
- Infrasound signals measured at the station I45RU can clearly be related to the 2017 event. It is the first time that a thermospheric propagation path of infrasound could be observed for an underground nuclear explosion.
- No immediate measurements of radionuclides related to the test in September were observable, but later occurrences of radionuclides are consistent with a delayed leakage from the test site in October.
- The test site might have been strongly stressed and shattered and ~~might be~~thus rendered useless for further test activities.

The combination of the results from the different technologies and methods yields a reliable estimation of hypocenter, magnitude, explosive energy, source mechanism as well as an indication for delayed leakage of ^{133}Xe from the test site. The cross-links between the different results complement each other in a consistent manner. The multi-technology and multi-methodology analysis presented in this study, clearly indicates that the September 2017 North Korean event was in fact a nuclear test. Even

in the phase of pre entry-into-force the CTBTO verification regime has again demonstrated its readiness with respect to the recent nuclear test.

Data. The facilities of IRIS Data Services, and specifically the IRIS Data Management Center, were used for access to seismic waveforms, related metadata, and/or derived products used in this study. IRIS Data Services arefunded through the Seismological Facilities for the Advancement of Geoscience and EarthScope (SAGE) Proposal of the National Science Foundation under Cooperative Agreement EAR-1261681. Seismic, infrasound and radionuclide data from stations of the IMS network (seismic, infrasound, radionuclide) were obtained by the German NDC through the IDC of the CTBTO. ECMWF operational analysis data is used for infrasound propagation modeling. ATM using HYSPLIT is operated with GDAS and GFS meteorological data from the United States NCEP. Satellite from ALOS-2 was obtained by GAF AG, data from the Pleiades satellite was delivered by Airbus Defence and Space.

Acknowledgements. The critical and helpful comments by Stefanie Donner (BGR) and Patrick Hupe (BGR) are highly appreciated. Furthermore we highly appreciate comments by Michael Ritzwoller (CU), ~~and~~ Jörg Renner (RUB), Felix M. Schneider (GFZ) as well as by ~~two~~three anonymous reviewers. NN acknowledges support from the German Federal Ministry of Education and Research in the context of the project SECURE (FKZ-03A0013A).

Author contributions. Authors contributions to the different Sections and Subsections of this study, including data analysis and interpretation, preparation of the figures and results, as well as writing, is as following: Subsection 2.1 Epicenter location: GH and PG. Subsection 2.2 Estimation of Hypocenter Depth and Seismic Moment: SC, TD, NN. Subsection 2.3 Moment Tensor Inversion of the Test and the Main Aftershock: AB, SC, and TD. Subsection 2.4 Magnitude and Yield Estimation: GH and PG. Subsection 2.5 Influence of the Mt. Mantap Topography: LC and PG. Section 3 Infrasound Observations: CP, KK, LC and PG. Section 4 Remote Sensing Studies: MF and IG. Section 5 Radionuclide Monitoring and Atmospheric Transport Modeling: OR and PG. PG, LC and TD devised and finalized the original manuscript.

Competing interests. The authors declare that they have no conflict of interest.

References

Adam, N., Parizzi, A., Eineder, M., and Crosetto, M.: Practical persistent scatterer processing validation in the course of the Terrafirma project, Journal of Applied Geophysics, 69, 59 – 65, https://doi.org/https://doi.org/10.1016/j.jappgeo.2009.07.002, advances in SAR Interferometry from the 2007 Fringe Workshop, 2009.

Arnold, L. and Pyne, K.: The First Trial — Grapple, pp. 131–150, Palgrave Macmillan UK, London, https://doi.org/10.1057/9780230599772_10, 2001.

Assink, J., Averbuch, G., Shani-Kadmiel, S., Smets, P., and Evers, L.: A Seismo-Acoustic Analysis of the 2017 North Korean Nuclear Test, Seismological Research Letters, https://doi.org/10.1785/0220180137, 2018.

Assink, J. D., Averbuch, G., Smets, P. S. M., and Evers, L. G.: On the infrasound detected from the 2013 and 2016 DPRK's underground nuclear tests, Geophysical Research Letters, 43, 3526–3533, https://doi.org/10.1002/2016GL068497, 2016.

Barth, A.: Significant release of shear energy of the North Korean nuclear test on February 12, 2013, Journal of Seismology, 18, 2014.

Bassin, C., Laske, G., and Masters, G.: The Current Limits of Resolution for Surface Wave Tomography in North America, Eos, 81, 2000.

Becker, A., Wotawa, G., De Geer, L.-E., Seibert, P., Draxler, R. R., Sloan, C., D'Amours, R., Hort, M., Glaab, H., Heinrich, P., Grillon, Y., Shershakov, V., Katayama, K., Zhang, Y., Stewart, P., Hirtl, M., Jean, M., and Chen, P.: Global backtracking of anthropogenic radionuclides by means of a receptor oriented ensemble dispersion modelling system in support of Nuclear-Test-Ban Treaty verification, Atmospheric Environment, 41, 4520–4534, https://doi.org/https://doi.org/10.1016/j.atmosenv.2006.12.048, 2007.

Bormann, P.: New Manual of Seismological Observatory Practice (NMSOP-2), Deutsches GeoForschungszentrum GFZ ; IASPEI, Potsdam, https://doi.org/10.2312/GFZ.NMSOP-2, 2012.

Boucher, G., Ryall, A., and Jones, A. E.: Earthquakes associated with underground nuclear explosions, Journal of Geophysical Research, 74, 3808–3820, https://doi.org/10.1029/JB074i015p03808, 1969.

Bowers, D., Marshall, P. D., and Douglas, A.: The level of deterrence provided by data from the SPITS seismometer array to possible violations of the Comprehensive Test Ban in the Novaya Zemlya region, Geophysical Journal International, 146, 425–438, https://doi.org/10.1046/j.1365-246x.2001.01462.x, 2001.

Cansi, Y.: An automatic seismic event processing for detection and location: The P.M.C.C. Method, Geophysical Research Letters, 22, 1021–1024, https://doi.org/10.1029/95GL00468, 1995.

Cesca, S. and Heimann, S.: Moment Tensor Solutions - A Useful Tool for Seismotectonics, chap. Challenges in regional moment tensor resolution and interpretation, Springer Natural Hazards, https://doi.org/10.1007/978-3-319-77358-2, 2017.

Cesca, S., Rohr, A., and Dahm, T.: Discrimination of induced seismicity by full moment tensor inversion and decomposition, Journal of Seismology, 17, 147–163, 2013.

Cesca, S., Heimann, S., Kriegerowski, M., Saul, J., and Dahm, T.: Moment Tensor Inversion for Nuclear Explosions: What Can We Learn from the 6 January and 9 September 2016 Nuclear Tests, North Korea?, Seismological Research Letters, 88, 300, https://doi.org/10.1785/0220160139, 2017.

Che, I.-Y., Park, J., Kim, I., Kim, T. S., and Lee, H.-I.: Infrasound signals from the underground nuclear explosions of North Korea, Geophysical Journal International, 198, 495–503, https://doi.org/10.1093/gji/ggu150, 2014.

CNN: North Korea blows up tunnels at Punggye-ri nuclear test site, https://edition.cnn.com/2018/05/24/asia/north-korea-nuclear-test-site-intl/index.html, 2018.

Coblentz, D. and Pabian, F.: Revised Geologic Site Characterization of the North Korean Test Site at Punggye-ri, Science & Global Security, 23, 101–120, 2015.

CTBTO: Preparatory Commission for the Comprehensive Nuclear-Test-Ban Treaty Organization, https://www.ctbto.org/, 2018.

Dahm, T. and Krüger, F.: New Manual of Seismological Observatory Practice (NMSOP-2), IASPEI, GFZ German Research Centre for Geosciences, Potsdam; http://nmsop.gfz-potsdam.de, chap. Moment tensor inversion and moment tensor interpretation, Deutsches GeoForschungsZentrum GFZ, Potsdam, Germany, https://doi.org/10.2312/GFZ.NMSOP-2_IS_3.9, 2014.

Dahm, T., Küger, F., Stammler, K., Klinge, K., Kind, R., Wylegalla, K., and Grasso, J.-R.: The 2004 Mw 4.4 Rotenburg, Northern Germany, Earthquake and Its Possible Relationship with Gas Recovery, Bulletin of the Seismological Society of America, 97, 691, https://doi.org/10.1785/0120050149, 2007.

Drob, D. P., Picone, J. M., and Garcés, M.: Global morphology of infrasound propagation, Journal of Geophysical Research, 108, 13–1–13–12, https://doi.org/10.1029/2002JD003307, 4680, 2003.

Evers, L. G. and Haak, H. W.: Infrasonic forerunners: Exceptionally fast acoustic phases, Geophysical Research Letters, 34, https://doi.org/10.1029/2007GL029353, l10806, 2007.

Ford, S. R., Dreger, D. S., and Walter, W. R.: Network Sensitivity Solutions for Regional Moment-Tensor Inversions, Bulletin of the Seismological Society of America, 100, 1962, https://doi.org/10.1785/0120090140, 2010.

Gaebler, P. J. and Ceranna, L.: Monitoring Compliance with the Comprehensive Nuclear-Test-Ban Treaty (CTBT). Contributions by the German National Data Center, chap. The Seismic Network of the International Monitoring System (IMS), pp. 69–90, Schweizerbart Science Publishers, Stuttgart, Germany, 2017.

Gatelli, F., Monti Guamieri, A., Parizzi, F., Pasquali, P., Prati, C., and Rocca, F.: The Wavenumber Shift in SAR Interferometry, 29, 855 – 865, 1994.

Gibbons, S. J., Pabian, F., Näsholm, S. P., Kværna, T., and Mykkeltveit, S.: Accurate relative location estimates for the North Korean nuclear tests using empirical slowness corrections, Geophysical Journal International, 208, 101–117, https://doi.org/10.1093/gji/ggw379, 2017.

Glasstone, S. and Dolan, P. J.: The Effects of Nuclear Weapons, U.S. Government Printing Office, 1977.

Gleyzes, M. A., Perret, L., and Kubik, P.: Pleiades System Architecture and Main Performances, ISPRS - International Archives of the Photogrammetry, Remote Sensing and Spatial Information Sciences, pp. 537–542, https://doi.org/10.5194/isprsarchives-XXXIX-B1-537-2012, 2012.

Gutenberg, B.: Amplitudes of P, PP, and S and magnitude of shallow earthquakes*, Bulletin of the Seismological Society of America, 35, 57, 1945a.

Gutenberg, B.: Magnitude determination for deep-focus earthquakes*, Bulletin of the Seismological Society of America, 35, 117, 1945b.

Han, L., Wu, Z., Jiang, C., and Liu, J.: Properties of three seismic events in September 2017 in the northern Korean Peninsula from moment tensor inversion, Science Bulletin, 62, 1569 – 1571, https://doi.org/https://doi.org/10.1016/j.scib.2017.11.007, 2017.

Hartmann, G., Barth, A., Ross, J. O., Grünberg, I., and Frei, M.: Monitoring Compliance with the Comprehensive Nuclear-Test-Ban Treaty (CTBT). Contributions by the German National Data Center, chap. Verification of the North Korean Nuclear Explosions 2006, 2009, 2013, and 2016, pp. 137–165, Schweizerbart Science Publishers, Stuttgart, Germany, 2017.

Heimann, S., Isken, M., Kühn, D., Sudhaus, H., Steinberg, A., Vasyura-Bathke, H., Daout, S., Cesca, S., and T., D.: Grond - A probabilistic earthquake source inversion framework. V. 1.0., GFZ Data Services, https://doi.org/https://doi.org/10.5880/GFZ.2.1.2018.003, 2018.

Hudson, J. A., Pearce, R. G., and Rogers, R. M.: Source type plot for inversion of the moment tensor, Journal of Geophysical Research: Solid Earth, 94, 765–774, https://doi.org/10.1029/JB094iB01p00765, 1989.

Kalinowski, M., Axelsson, A., Bean, M., Blanchard, X., Bowyer, T., Brachet, G., Hebel, S., McIntyre, J., Peters, J., Pistner, C., Raith, M., Ringbom, A., R. J. Saey, P., Schlosser, C., J. Stocki, T., Taffary, T., and Ungar, K.: Discrimination of Nuclear Explosions against Civilian Sources Based on Atmospheric Xenon Isotopic Activity Ratios, Pure and Applied Geophysics, 167, 517–539, 2010.

Kampes, B. M.: Radar Interferometry – Persistent Scatterer Technique, Springer Netherlands, https://doi.org/10.1007/978-1-4020-4723-7, 2006.

Kennett, B. L. N., Engdahl, E. R., and Buland, R.: Constraints on seismic velocities in the Earth from traveltimes, Geophysical Journal International, 122, 108–124, https://doi.org/10.1111/j.1365-246X.1995.tb03540.x, 1995.

Koch, K. and Pilger, C.: Infrasound observations from the site of past underground nuclear explosions in North Korea, Geophysical Journal International, p. ggy381, https://doi.org/10.1093/gji/ggy381, 2018.

Korean Central News Agency: DPRK Nuclear Weapons Institute on Successful Test of H-bomb for ICBM, press release. Pyongyang September 3rd 2017., http://www.kcna.kp/, 2017.

Korean Meterological Agency: http://www.weather.go.kr/weather/earthquake_volcano/domesticlist.jsp?startTm=2017-09-01&endTm=2018-12-13&startSize=999&endSize=999&startLat=41.2&endLat=41.4&startLon=129&endLon=129.2&lat=&lon=&dist=&keyword=&x=36&y=11, 2018.

Le Pichon, A., Blanc, E., and Hauchecorne, A.: Infrasound Monitoring for Atmospheric Studies, Springer, https://doi.org/10.1007/978-1-4020-9508-5, 2010.

Liu, J., Li, L., Zahradník, J., Sokos, E., Liu, C., and Tian, X.: North Korea's 2017 Test and its Nontectonic Aftershock, Geophysical Research Letters, 45, 3017–3025, https://doi.org/10.1002/2018GL077095, 2018.

Massonnet, D., Rossi, M., Carmona, C., Adragna, F., Peltzer, G., Feigl, K., and Rabaute, T.: The displacement field of the Landers earthquake mapped by radar interferometry, Nature, 364, 138–142, https://doi.org/doi:10.1038/364138a0, 1993.

Murphy, J. R.: Identification of Seismic Sources — Earthquake or Underground Explosion, chap. P Wave Coupling of Underground Explosions in Various Geologic Media, pp. 1201–205, Springer Netherlands, Dordrecht, https://doi.org/10.1007/978-94-009-8531-5, 1981.

Mutschlecner, J. P. and Whitaker, R. W.: Infrasound from earthquakes, Journal of Geophysical Research: Atmospheres, 110, 2005.

Nuclear Safety and Security Commission: Press Release: Radionuclide Detection After the 6th North Korea Nuclear Test, http://www.nssc.go.kr/_custom/nssc/_common/board/download.jsp?attach_no=20247, 2017.

Pabian, F. and Coblentz, D.: Surface Disturbances at the Punggye-ri Nuclear Test Site: Another Indicator of Nuclear Testings?, Los Alamos National Laboratory. Report posted on 38north.org, final version issued March 15, 2017, 2017.

Park, J., Che, I.-Y., Stump, B., Hayward, C., Dannemann, F., Jeong, S., Kwong, K., McComas, S., Oldham, H. R., Scales, M. M., and Wright, V.: Characteristics of infrasound signals from North Korean underground nuclear explosions on 2016 January 6 and September 9, Geophysical Journal International, 214, 1865–1885, 2018.

Pilger, C., Ceranna, L., and Bönnemann, C.: Monitoring Compliance with the Comprehensive Nuclear-Test-Ban Treaty (CTBT). Contributions by the German National Data Center, Schweizerbart Science Publishers, Stuttgart, Germany, 2017.

Ringbom, A., Axelsson, A., Aldener, M., Auer, M., Bowyer, T., Fritioff, T., Hoffman, I., Khrustalev, K., Nikkinen, M., Popov, V., Popov, Y., Ungar, K., and Wotawa, G.: Radioxenon detections in the CTBT international monitoring system likely related to the announced nuclear test in North Korea on February 12, 2013, Journal of Environmental Radioactivity, 128, 47 – 63, https://doi.org/https://doi.org/10.1016/j.jenvrad.2013.10.027, 2014.

Ringdal, F., Marshall, P. D., and Alewine, R. W.: Seismic yield determination of Soviet underground nuclear explosions at the Shagan River test site, Geophysical Journal International, 109, 65–77, https://doi.org/10.1111/j.1365-246X.1992.tb00079.x, 1992.

Ross, J. O., Bollhöfer, A., and Schlosser, C.: Monitoring Compliance with the Comprehensive Nuclear-Test-Ban Treaty (CTBT). Contributions by the German National Data Center, chap. The IMS Radionuclide Network Supported by Atmospheric Transport Modelling (ATM), pp. 123–136, Schweizerbart Science Publishers, Stuttgart, Germany, 2017.

Stein, A. F., Draxler, R. R., Rolph, G. D., Stunder, B. J. B., Cohen, M. D., and Ngan, F.: NOAA's HYSPLIT Atmospheric Transport and Dispersion Modeling System, Bulletin of the American Meteorological Society, 96, 2059–2077, https://doi.org/10.1175/BAMS-D-14-00110.1, 2015.

Suzuki, S., Osawa, Y., Hatooka, Y., Kankaku, Y., and Watanabe, T.: Overview of Japan's Advanced Land Observing Satellite-2 mission, https://doi.org/10.1117/12.831340, 2009.

Tessmer, E., Kosloff, D., and Behle, A.: Elastic wave propagation simulation in the presence of surface topography, Geophysical Journal International, 108, 621–632, https://doi.org/10.1111/j.1365-246X.1992.tb04641.x, 1992.

Vavryčuk, V. and Kim, S. G.: Nonisotropic radiation of the 2013 North Korean nuclear explosion, Geophysical Research Letters, 41, 7048–7056, https://doi.org/10.1002/2014GL061265, 2014.

Waldhauser, F. and Ellsworth, W. L.: A Double-Difference Earthquake Location Algorithm: Method and Application to the Northern Hayward Fault, California, Bulletin of the Seismological Society of America, 90, 1353–1368, https://doi.org/10.1785/0120000006, 2000.

Wang, R.: A simple orthonormalization method for stable and efficient computation of Green's functions, Bulletin of the Seismological Society of America, 89, 733, 1999.

Wang, T., Shi, Q., Nikkhoo, M., Wei, S., Barbot, S., Dreger, D., Bürgmann, R., Motagh, M., and Chen, Q.-F.: The rise, collapse, and compaction of Mt. Mantap from the 3 September 2017 North Korean nuclear test, Science, https://doi.org/10.1126/science.aar7230, 2018.

Wei, M.: Location and source characteristics of the 2016 January 6 North Korean nuclear test constrained by InSAR, Geophysical Journal International, 209, 762–769, https://doi.org/10.1093/gji/ggx053, 2017.

Zhang, M. and Wen, L.: High-precision location and yield of North Korea's 2013 nuclear test, Geophysical Research Letters, 40, 2941–2946, https://doi.org/10.1002/grl.50607, 2013.

Zhao, L., Xie, X., Wang, W., and Yao, Z.: The 12 February 2013 North Korean Underground Nuclear Test, Seismological Research Letters, 85, 130–134, https://doi.org/10.1785/0220130103, 2014.

Zhao, L.-F., Xie, X.-B., Wang, W.-M., Hao, J.-L., and Yao, Z.-X.: Seismological investigation of the 2016 January 6 North Korean underground nuclear test, Geophysical Journal International, 206, 1487–1491, https://doi.org/10.1093/gji/ggw239, 2016.

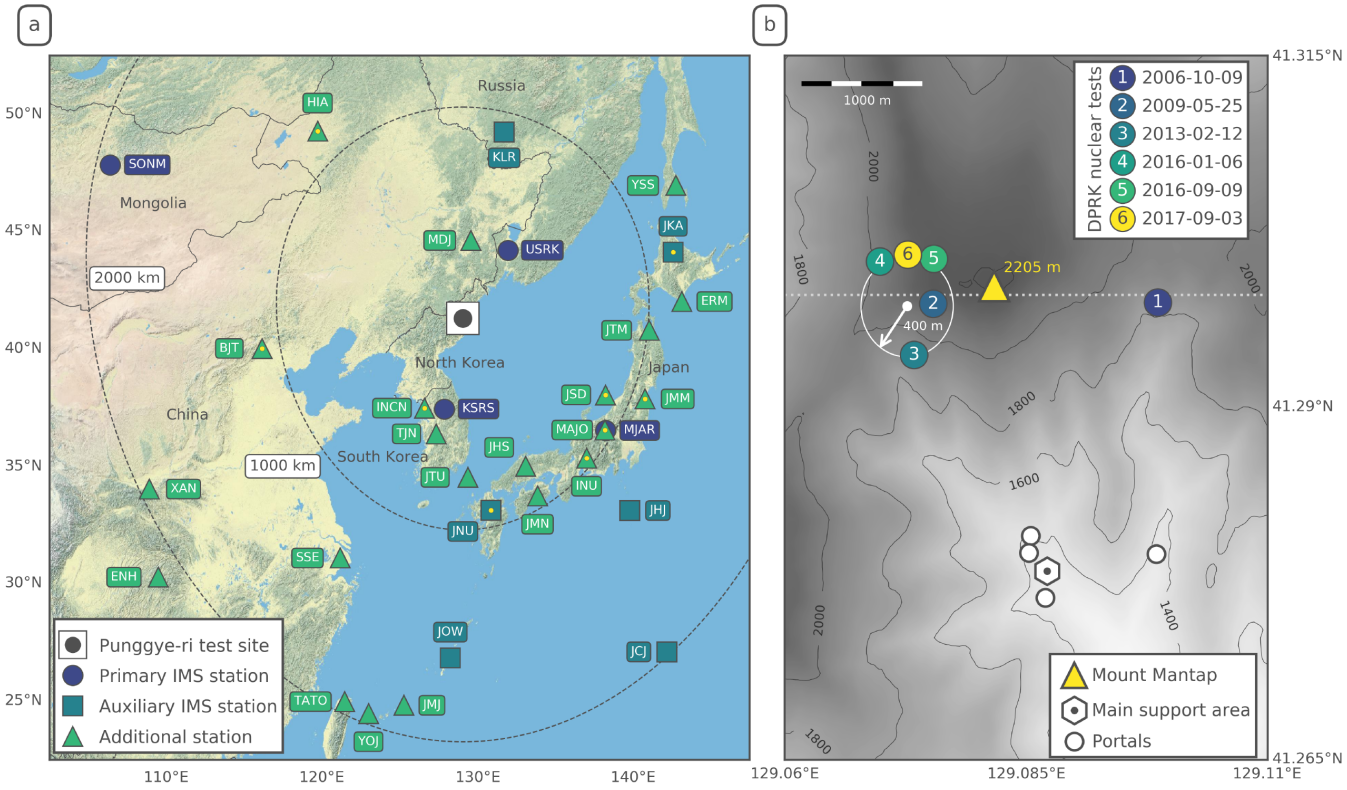

Figure 1. (a) Seismic stations of the International Monitoring System and other earthquake monitoring networks within a radius of 2100 km from the North Korean Punggye-ri nuclear test site. Stations that are used in the moment tensor analysis in Subsection 2.3 are marked with a small yellow dot. (b) Zoom into the Punggye-ri test site area. Numbered circles indicate the absolute locations of the six North Korean nuclear tests. The relative location error for each test is less than 100 m. Dashed line marks the profile used in Subsection 2.5 to study of topographic influence of the Mt. Mantap on seismic energy generation and radiation from the test.

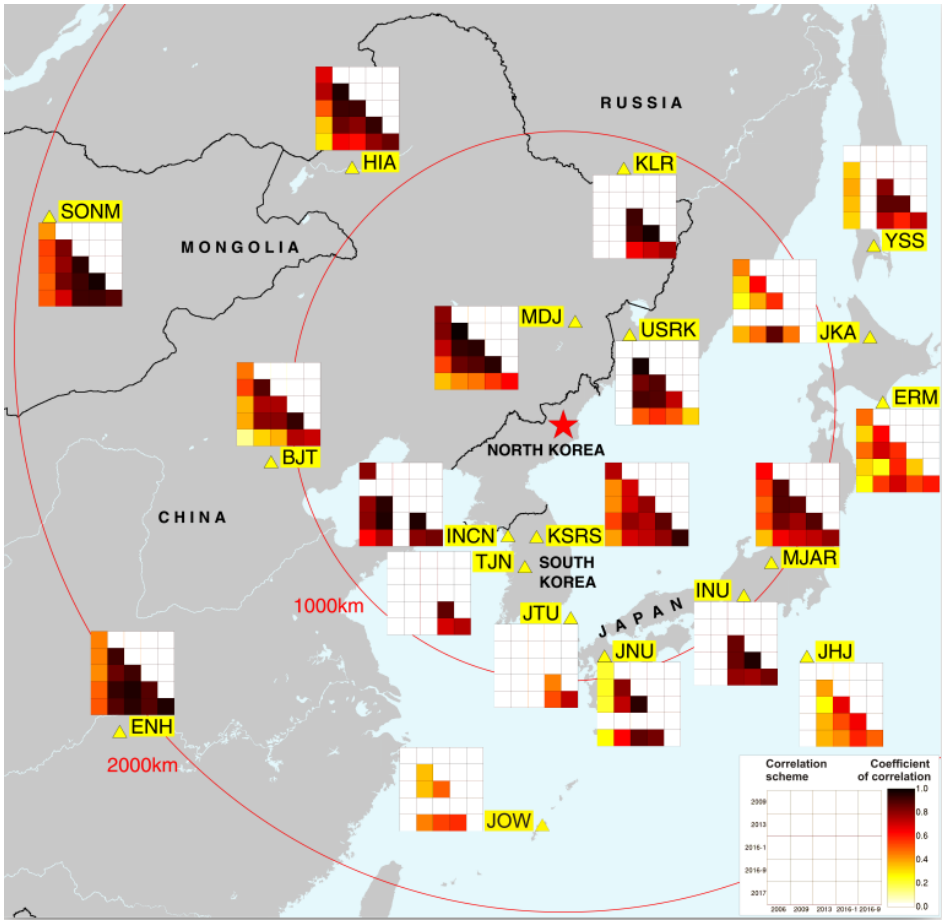

Figure 2. Maximum correlation coefficients for the coherence of the Pn-phase for all available pairs of nuclear tests at 18 stations in regional distances of up to 2100 km. Due to their similar size in explosive yield, the four tests in the years 2009, 2013 and 2016 have a similar source mechanism and consequently show high maximum correlation coefficients between 0.70 and 0.99. The seismic signals for the 2006 and 2017 test are in general less correlated with the other tests due to the different source durations suspected for these two events. The 2006 and 2017 are the smallest and largest explosion, respectively.

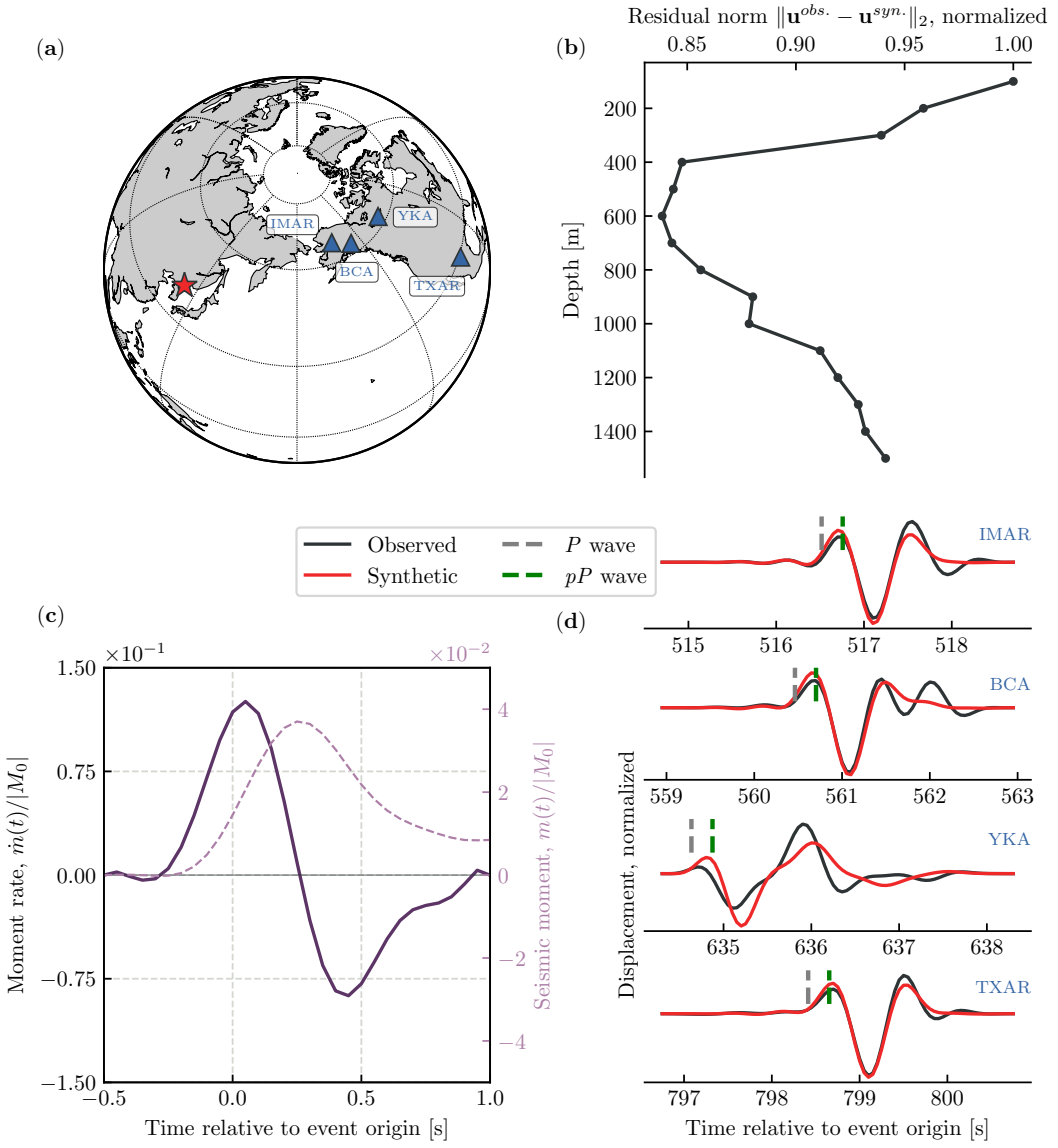

Figure 3. (a) Setup of the depth analysis with the 2017 North Korean nuclear test marked as red star and the four small-aperture, short-period arrays marked as bluish triangles. The epicentral distances to arrays IMAR, BCA, YKA and TXAR are 48°, 54°, 65° and 94°, respectively. (b) Residuals between observed and synthetic waveforms (L_2-norm) as a function of depth of the explosion. (c) Least squares source time function associated with the best-fit regularized solution. Solid and dashed lines are the normalized moment rate and moment function, respectively. (d) Observed (black) and synthetic (red) waveforms for the best-fit regularized solution at 600 m depth. The gray and green dashed lines indicate the theoretical arrival times of the P-and pP-phases, respectively. The traces are bandpass-filtered between 0.5 and 2.5 Hz.

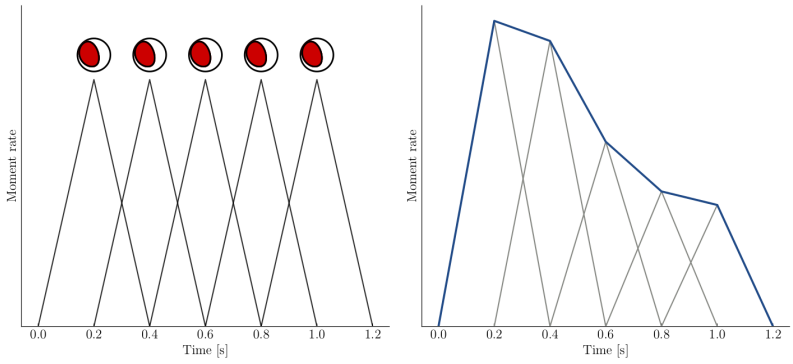

Figure 4. (Left): Schematic sketch of five triangular basis functions $h_l(t)$ with equal weight of 1 and with a duration of 0.4 s each. The focal sphere symbols indicate that the orientation of the source mechanism is assumed constant during the rupture process. (Right): Simulation of a complex moment rate function (blue line) by applying different weights to h_l and linear superposition.

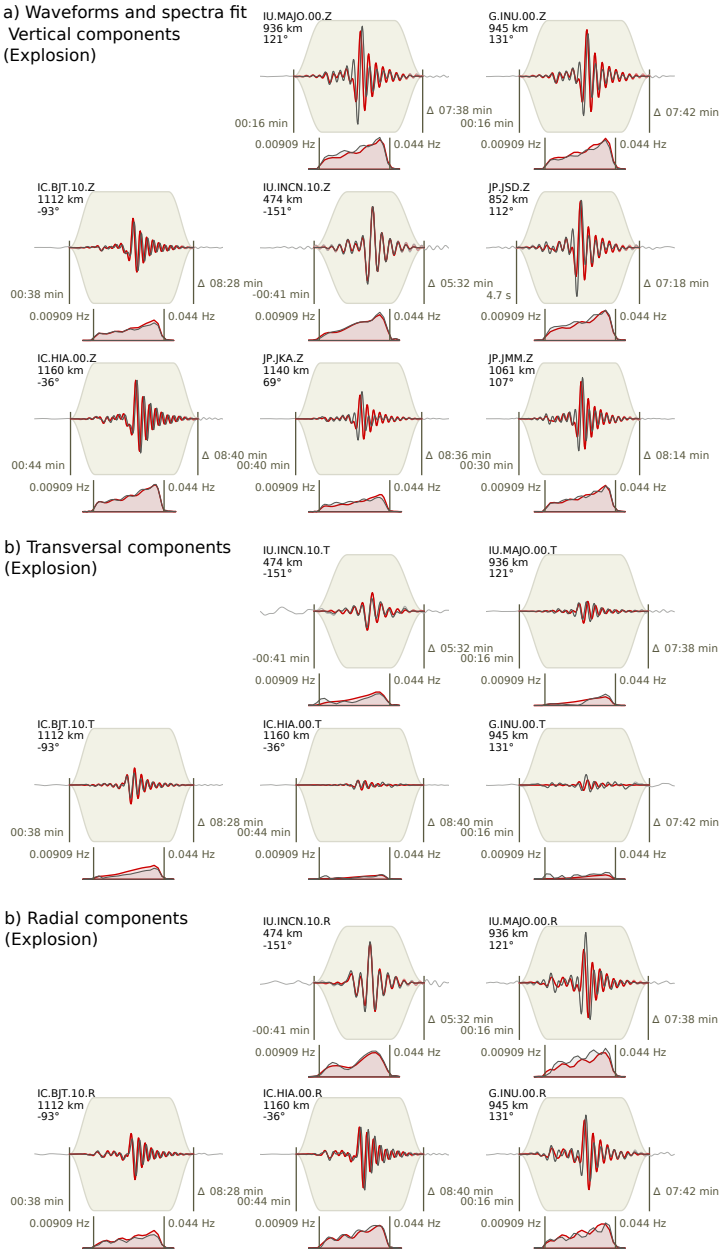

Figure 5. Full waveform displacement and amplitude spectra fits (gray and red lines denote observations and synthetics, respectively) are shown for the nuclear explosion for the vertical (a), transversal (b), and radial components (c). Top left side of each plot reports the trace component (network, station, location, and component codes), epicentral distance, and azimuth. Waveform plots report the starting time (relative to the origin time) and duration (in minutes and seconds) of the time window used (the gray background represents the applied taper), while spectra plots report the frequency range in Hz. For geographical locations of the used stations see Figure 1a.

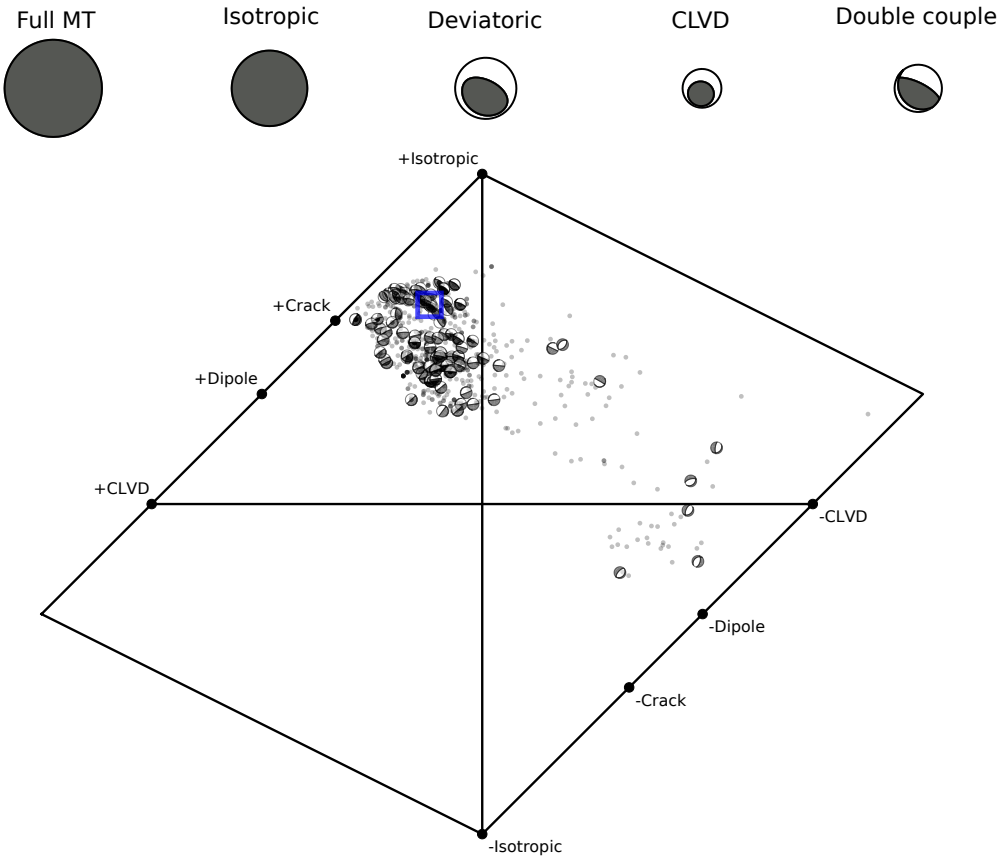

Figure 6. Best moment tensor decomposition (top) and source type plots (bottom) for the 2017 explosion. Top: The moment tensor decompositions reports the focal sphere for the full moment tensor, and its isotropic and deviatoric components. The deviatoric component is further decomposed into CLVD and DC terms. The relative size of focal spheres scale with their relative magnitude. Bottom: The source type diagram after Hudson et al. (1989) is used to judge the moment tensor decomposition, illustrating the ensemble of best fitting solutions. Figure shows both solutions based on all available data, as well as using data subsamples upon bootstrapping ~~(circles, focal spheres for the DC components are shown for selected solutions only)~~. The position of each solution (circles, focal sphere for selected solutions) illustrates the MT decomposition, while the focal spheres (shown for selected solutions only) illustrate the geometry of the DC term. The decomposition of the best solution is denoted by a blue square.

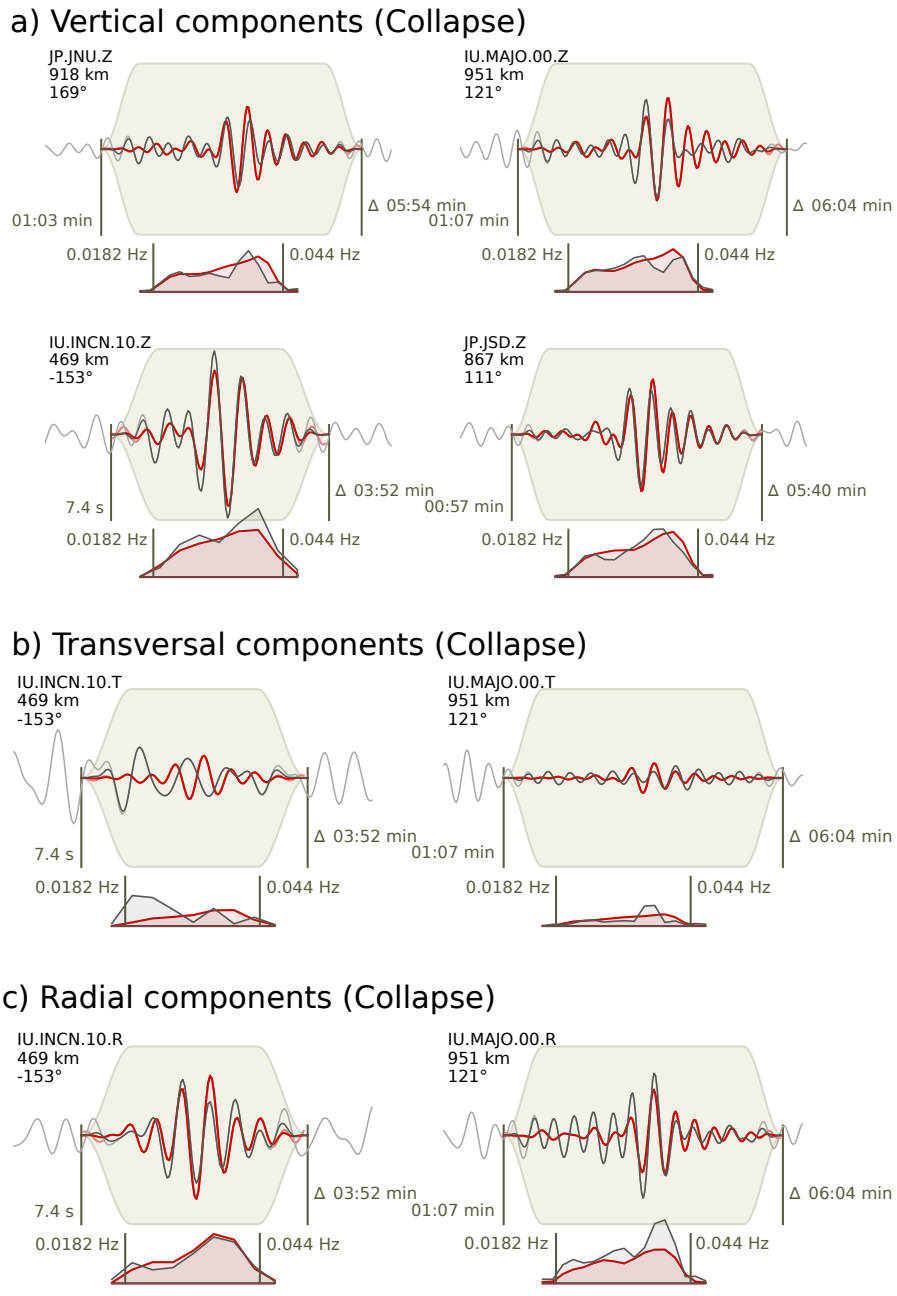

Figure 7. Same as Figure 5, but for the aftershock around eight minutes after the test.

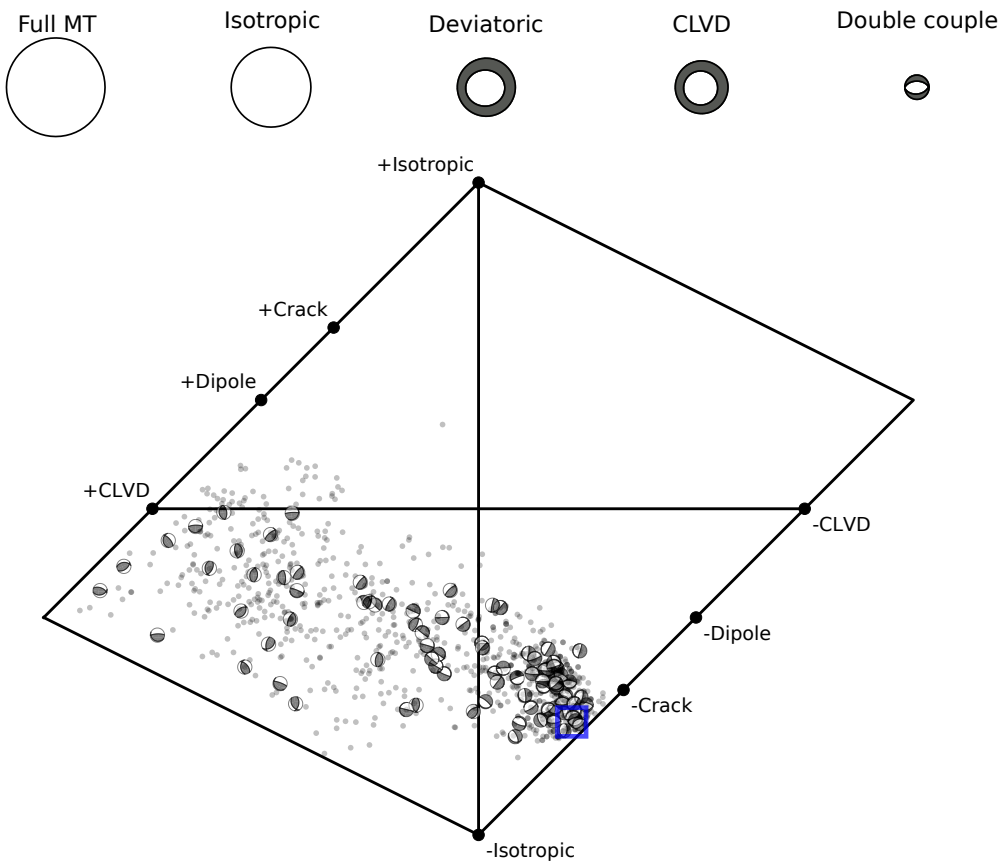

Figure 8. Same as Figure 6, but for the aftershock around eight minutes after the underground test.

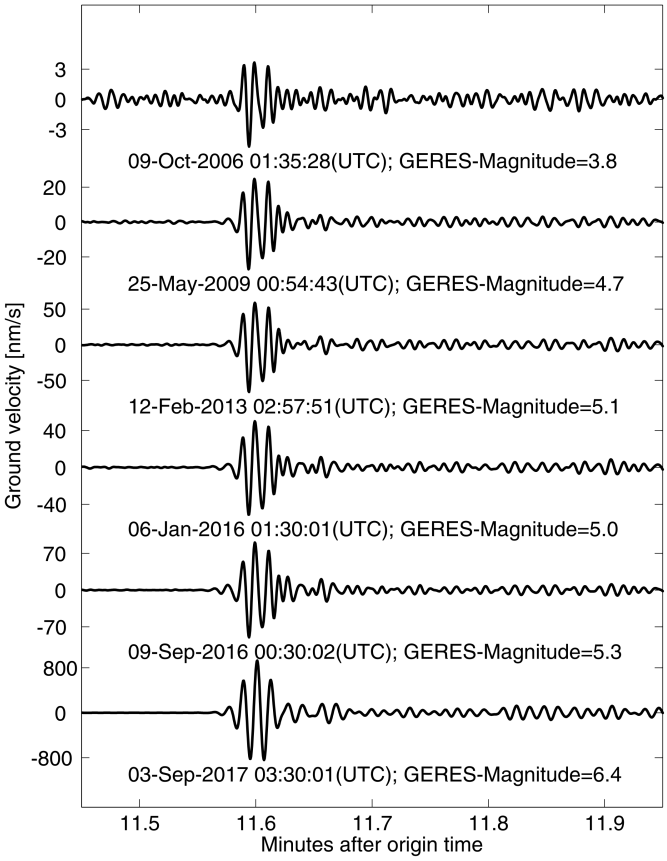

Figure 9. Beam seismograms calculated from the vertical components of the GERES array showing the P-wave of the six North Korean nuclear explosions. The seismograms are normalized to the individual maximum amplitudes, for which the station magnitude is estimated.

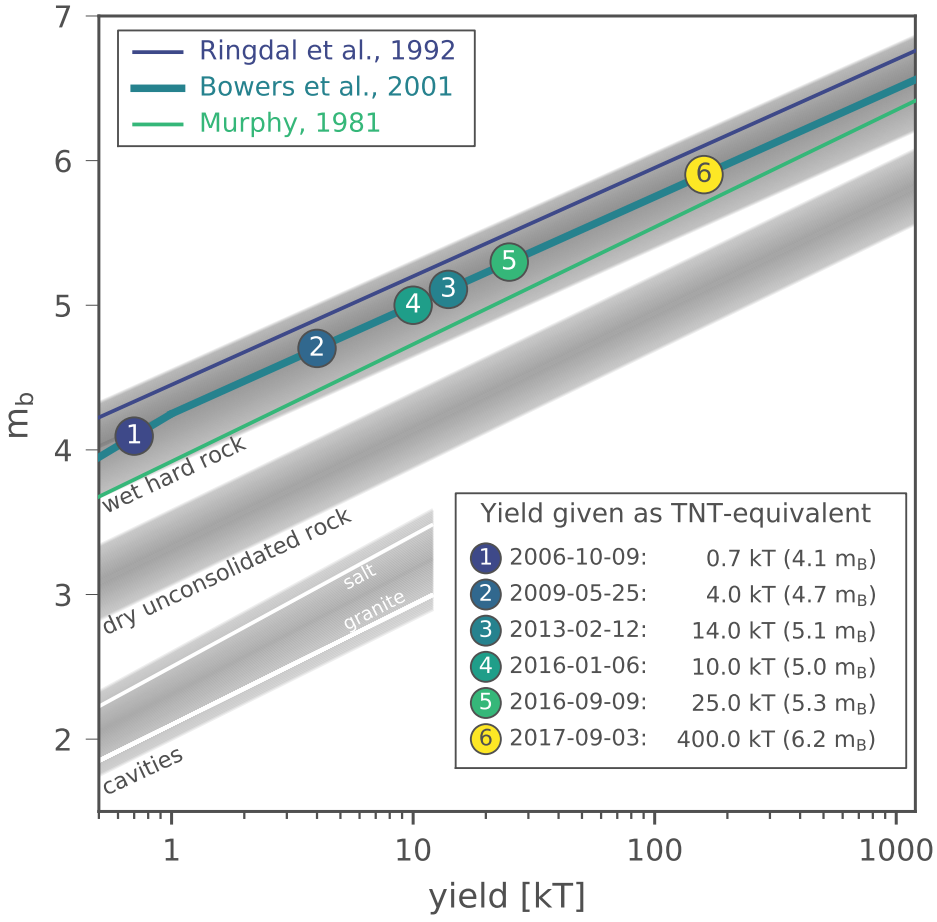

Figure 10. Magnitude-yield relation curves for different geological settings. Numbered circles indicate the six North Korean nuclear tests. Gray background shading represents lower and upper boundary literature values for the different environments.

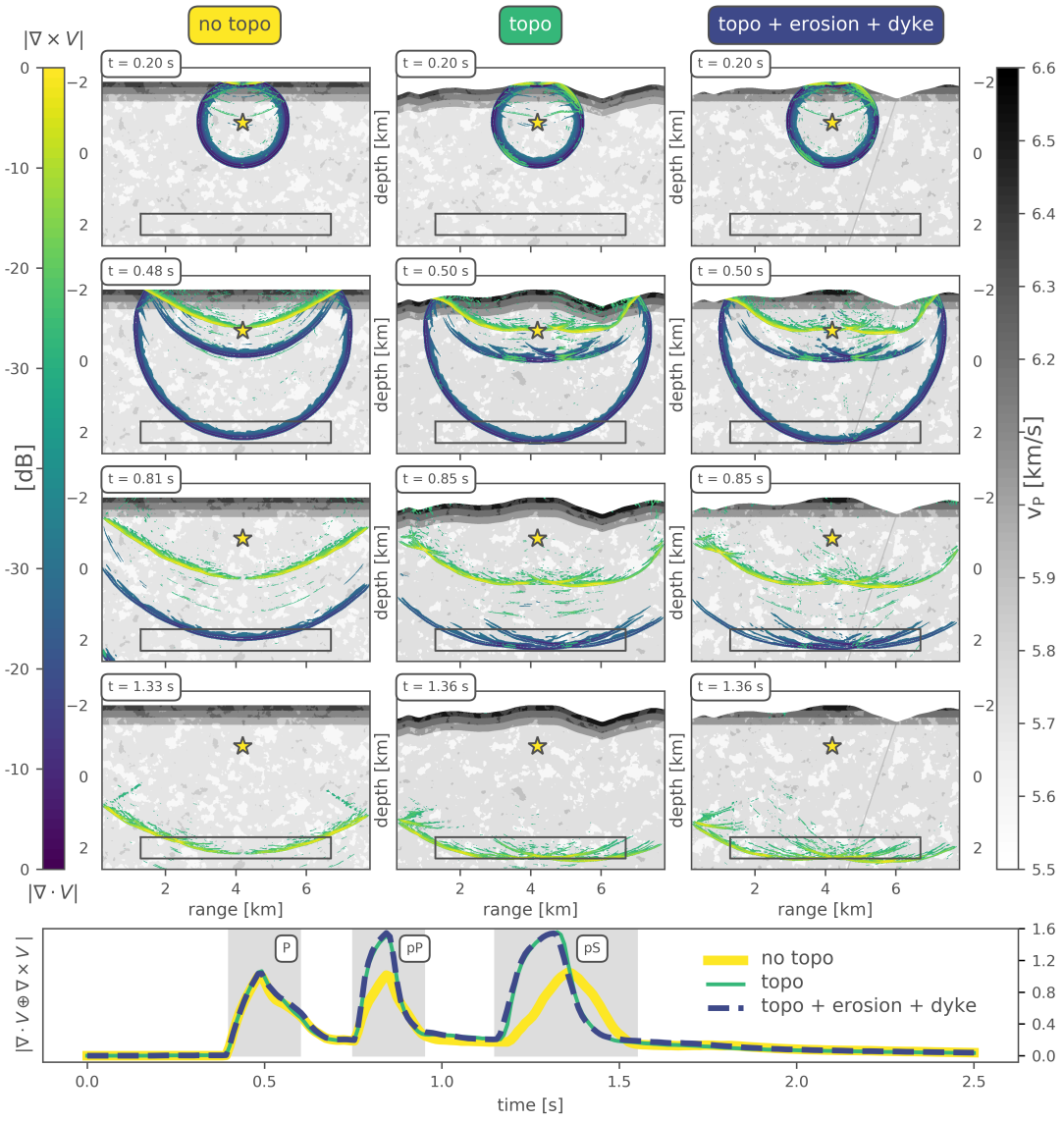

Figure 11. Snapshots obtained by and velocity model used for numerical simulations. P-wave velocities are indicated by shading according to the gray scale map (for S-wave velocities we assume a v_P/v_S-ratio of 1.73), as well as logarithmically scaled divergence (P-wave energy) and curl (SV-wave energy) by bluish and greenish colors, respectively. The left paneled snapshots show the P- and SV-wave separated propagation for an explosion source without topography, the middle panels with topography across the North Korean test site for a West-East profile along 41.3°N with Mt. Mantap in the middle. The right panel shows is similar to the middle panel, but with a more realistic geological setting, where erosion is accounted for. The time stamp of each snapshot is displayed in the upper left corner. The point source is beneath the center of Mt. Mantap in a depth of 0.6 km below surface. The panel below the snapshots compares the summed average divergence and curl computed every 0.02 s in a rectangular box below the source for the case without (yellow) and the cases with (green and blue) topography. The downward propagating wave-field shows strongly increased amplitudes for pP- and pS-phases in both cases of topography.

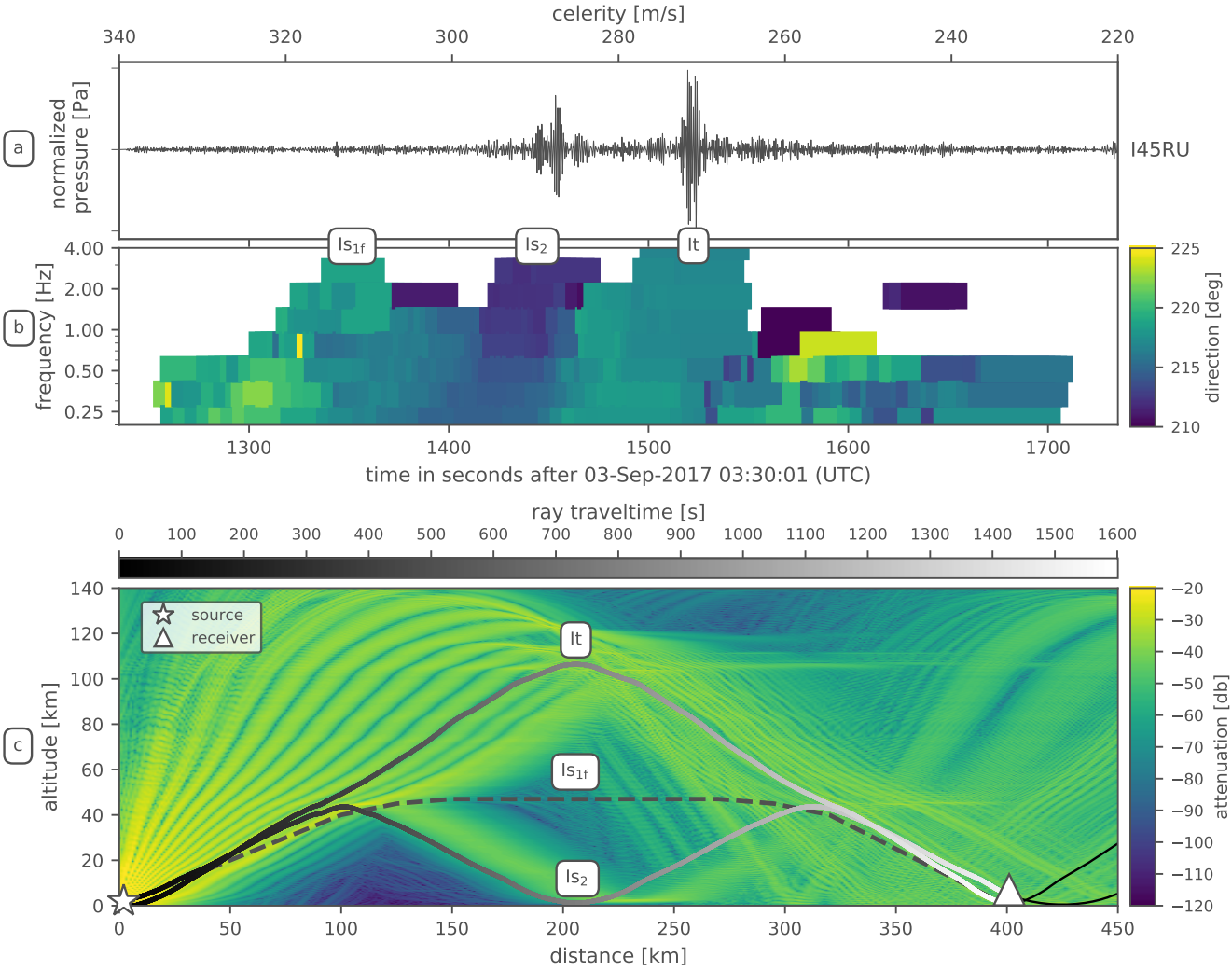

Figure 12. (a) Waveform beam of the 4-element infrasound array I45RU with corresponding celerity values. (b) Progressive Multi-Channel Correlation analysis in the same time frame for signal frequencies between 0.2 and 4 Hz. Information on back-azimuth direction is color coded. True back-azimuth from test site to station is 218°. (c) Propagation modeling using raytracing with gray-shaded travel-time information for eigenrays from the test site to the station and color coded attenuation information from parabolic equation modeling. Is_2 and It denote the corresponding stratospheric and thermospheric arrivals~~.~~ after 1450 s and 1520 s, respectively. Is_{1f} shows the early signal detection and theoretical raypath for an infrasonic forerunner.

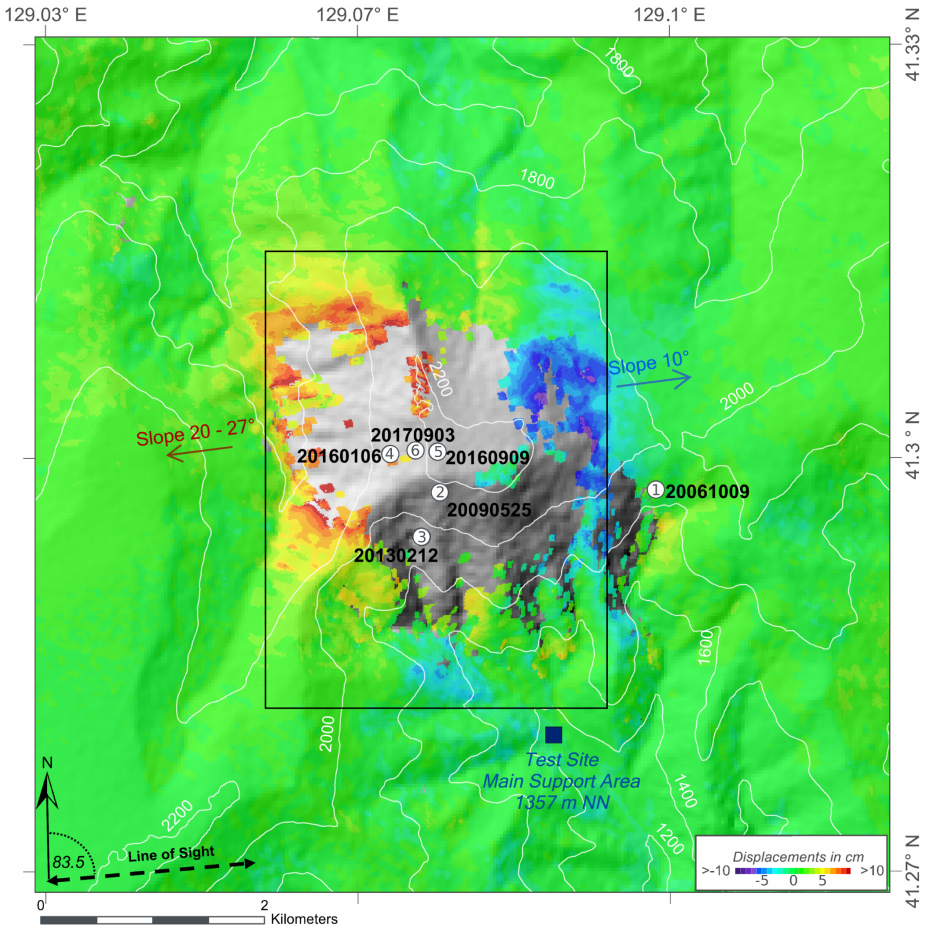

Figure 13. Surface displacements from DINSAR analysis for the 2017 North Korean nuclear test in September 2017. Coherence threshold is set to 0.25. Data from the days August 29th and from September 12th 2017 are used. Arrows indicate slope direction and angle. Numbered circles indicate the epicenters of the tests from 2006 to 2017. Black solid box delineates an area of around 3×4 km^2 in which the surface displacement is between between -10 and 10 cm.

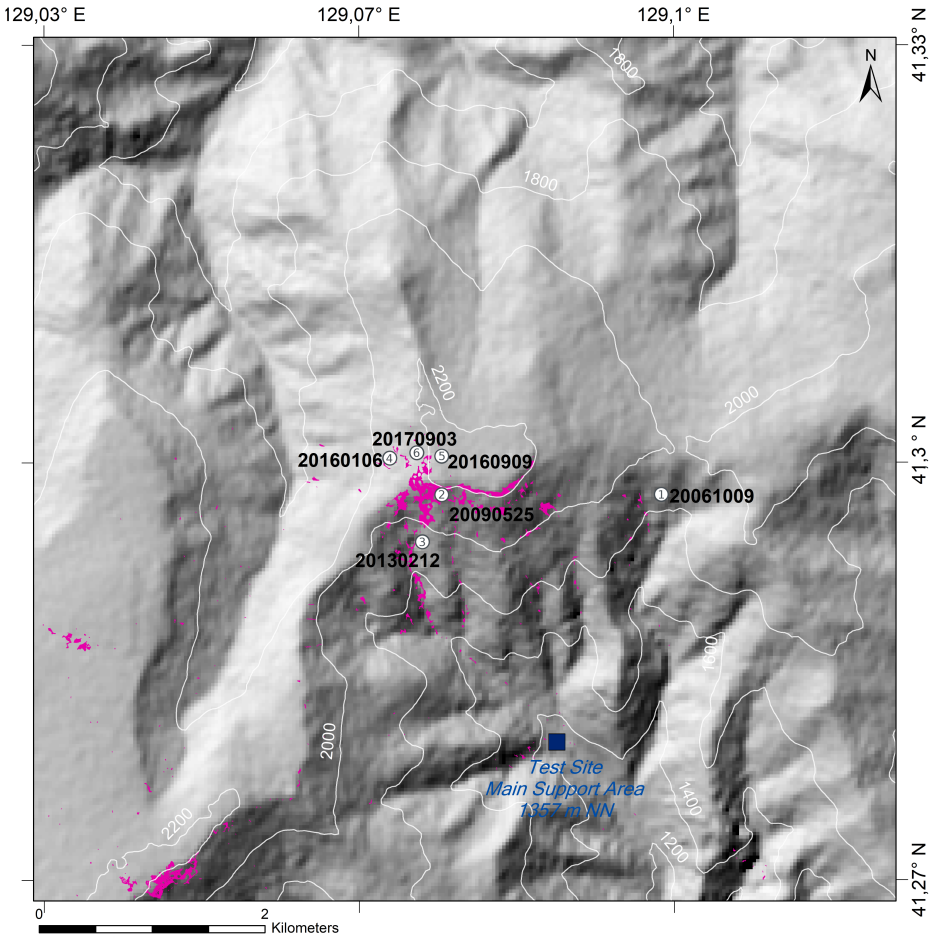

Figure 14. Change detection analysis via NDVI (Normalized Difference Vegetation Index) from Pleiades data showing potential landslides (in purple patches) triggered by the 2017 nuclear test. Numbered circles indicate the epicenters of the tests from 2006 to 2017.

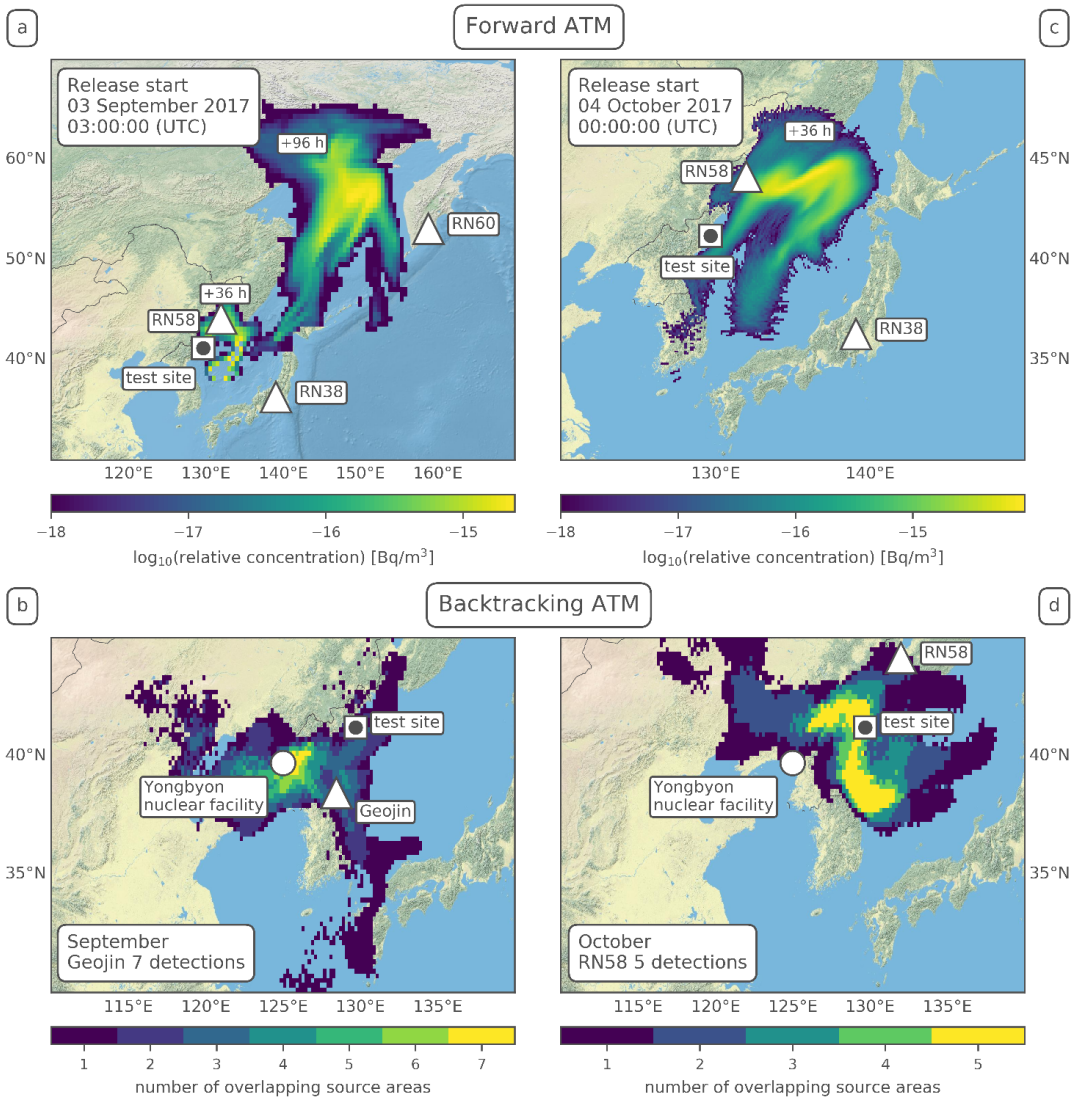

Figure 15. Atmospheric Transport Modeling results. (a) Forward dispersion modeling after 36 and 96 hours for an immediate release on September 3rd 2017. (b) Number of overlapping backward plumes for seven ^{133}Xe detecting samples in north-eastern South Korea from September 7th to 10th 2017 (fixed to 42 hours transport time for each sample). (c) High resolution forward dispersion modeling after 36 hours for a delayed leakage on October 4th 2017. (d) Number of overlapping backward plumes for five ^{133}Xe detecting samples at RN58 Ussurysk during October 2017 (transport time fixed at maximum sensitivity to North Korean test site).